1C02a

June 12, 2002
FINAL REPORT

VALIDATION OF 1-D NUMERICAL SIMULATION PROCEEDURES

A PEARL REPORT

to

PG&E/CEC/Caltrans

by

Walter Silva
Nick Gregor
Bob Darragh

of

Pacific Engineering and Analysis
311 Pomona Avenue
El Cerrito, CA 94530

TABLE OF CONTENTS

Section		Page
1.	INTRODUCTION	1
2.	STOCHASTIC FINITE-FAULT MODEL	1
3.	EARTHQUAKES, SITES, PROFILES, AND SLIP MODELS	1
	3.1 Chi-Chi, Taiwan Earthquake	1
	3.2 Kocaeli And Duzce, Turkey Earthquakes	2
4.	MODELING RESULTS	2
	4.1 Chi-Chi, Taiwan Earthquake	3
	4.2 Turkey Earthquakes	3
5.	REFERENCES	5

APPENDIX A – STOCHASTIC GROUND MOTION MODEL DESCRIPTION

APPENDIX B – SITE RESPONSE ANALYSIS METHOD

LIST OF TABLES

Table Number		Page
Table 1.	Crustal Models	7
Table 2.	Chi-Chi Earthquake Sites	8
Table 3.	Chi-Chi Earthquake Site Category Mapping	12
Table 4.	Kocaeli Earthquake Sites	13
Table 5.	Duzce Earthquake Sites	14
Table 6.	Finite Source Model Parmeters	15

LIST OF FIGURES

Figure Number		Page
Figure 1.	Shallow shear-wave velocity profiles used at rock and soil sites for the Chi-Chi, Taiwan earthquake. Profiles were placed on top of the regional crustal model (Table 1).	16
Figure 2.	Shallow shear-wave velocity profiles used at rock and soil sites for the Kocaeli and Duzce, Turkey earthquake. Profiles were placed on top of the regional crustal model (Table 1).	17
Figure 3.	Relative slip models used for the Chi-Chi, Taiwan and Kocaeli and Duzce, Turkey earthquakes.	18
Figure 4a.	Model bias computed for the Chi-Chi, Taiwan earthquake using base case parameters: all 139 sites within a 50 km rupture distance (Table 2).	19
Figure 4b.	Model variability computed for the Chi-Chi, Taiwan earthquake using base case parameters: all 139 sites within a 50 km rupture distance (Table 2).	20
Figure 5a.	Model bias computed for the Chi-Chi, Taiwan earthquake using base case parameters: all 41 sites within a 20 km rupture distance (Table 2).	21
Figure 5b.	Model bias computed for the Chi-Chi, Taiwan earthquake using base case parameters: all 41 sites within a 20 km rupture distance (Table 2).	22
Figure 6a.	Model bias computed for the Kocaeli, Turkey earthquake using base case parameters: all 34 sites (Table 4).	23
Figure 6b.	Model variability computed for the Kocaeli, Turkey earthquake using base case parameters: all 34 sites (Table 4).	24
Figure 7a.	Model bias computed for the Kocaeli, Turkey earthquake using base case parameters: all 15 sites within a 50 km rupture distance (Table 4).	25
Figure 7b.	Model variability computed for the Kocaeli, Turkey earthquake using base case parameters: all 15 sites within a 50 km rupture distance (Table 4).	26
Figure 8a.	Model bias computed for the Duzce, Turkey earthquake using base case parameters: all 22 sites (Table 5).	27
Figure 8b.	Model variability computed for the Duzce, Turkey earthquake using base case parameters: all 22 sites (Table 5).	28

LIST OF FIGURES

Figure Number		Page
Figure 9a.	Model bias computed for the Duzce, Turkey earthquake using base case parameters: all 12 sites within a 50 km rupture distance (Table 5).	29
Figure 9b.	Model variability computed for the Duzce, Turkey earthquake using base case parameters: all 12 sites within a 50 km rupture distance (Table 5).	30

1. INTRODUCTION

The objective of this project is to evaluate the ability of existing numerical simulation procedures to model the strong ground motions from the 1999 Chi-Chi, Taiwan as well as the Kocaeli and Duzce, Turkey earthquakes.

The simulation procedure implemented here is termed the stochastic finite fault model (Silva et al., 1990; 1997) in which near surface (top 100 to 1,000 ft) materials are considered in detail through an equivalent-linear formulation.

In the course of this project, a simulated annealing inversion algorithm was developed for determining a best-fit slip model, subevent rise time (Section 2.0), and rupture velocity. The desire was to develop these parameters in an optimum manner within the context of the wave propagation and rupture dynamics incorporated in the model, all including detailed nonlinear site response. However, the inversion code proved so time consuming (1 week for an inversion) on a 1.2 GHz PC that insufficient time was available to adequately test the algorithm and apply appropriate parameter constraints. As a result, slip models determined using an alternative wave propagation approach as well as rupture dynamics (spatially variable rise time and rupture velocity) were used.

2. STOCHASTIC FINITE-FAULT MODEL

The stochastic finite-fault model implemented here is quite simple in concept, using a single-corner-frequency omega-square source spectrum (**M** = 5.0) for each subfault. Large earthquakes are simulated by simply delaying and summing contributions from the **M** 5 subfaults. The process is discussed in detail in Appendix A. The model is simple, includes a frequency domain random vibration theory equivalent-linear site response (Appendix B) implemented for both rock and soil sites (Silva et al., 1997). The model, including site effects, has recently been validated at about 500 sites for 15 earthquakes (**M** 5.2 to 7.4) over fault distances ranging from 1 km to 470 km (Silva et al., 1997) and for subduction zone earthquakes for **M** up to 8.1. In general, the model is unbiased over the frequency range of recorded motions (spectral acceleration averaging from about 0.3 to 100 Hz).

3. EARTHQUAKES, SITES, PROFILES, AND SLIP MODELS

Three large recently occurring earthquakes were modeled: the 1999 **M** 7.6 Chi-Chi, Taiwan as well as both of the 1999 Turkey earthquakes: the **M** 7.4 Kocaeli and the **M** 7.1 Duzce. Table 1 lists the regional crustal and Q(f) models used in modeling the earthquakes. To model the effects of the shallow geotechnical layer on the predicted motions, generic rock and deep firm soil profiles were placed on top of the regional models (Table 1). Small strain kappa values (Appendix A) were set to 0.04 sec, base case values for both deep soil and soft rock implied by the Abrahamson and Silva (1997) and Sadigh et al. (1997) empirical attenuation relations (Silva et al., 1997; EPRI, 1993).

3.1 Chi-Chi, Taiwan Earthquake

For the Chi-Chi, Taiwan sites, soft rock and deep soil generic profiles, based primarily on shear-wave velocities measured at strong motion recording sites located in California, were used. These soft rock and deep soil (1,000 ft) profiles correspond to Geomatrix site categories A and B for rock and C and D for soil. The sites, categories, and rupture distances are listed in Table 2,

along with the category definitions. For these sites, both the Taiwan Central Weather Bureau (CWB, Table 2) qualitative and quantative NEHRP categories were available. Since few of the sites had available measured shear-wave velocity profiles, innovative indirect methods were used to assign NEHRP categories (Lee et al., 2001). Unfortunately the results using this approach were not without ambiguities, resulting in a number of apparent conflicts with the qualitative, largely visual CWB site categorization scheme. As a result, Table 3 was developed to provide a mechanism for consistently assigning either soft rock or deep firm soil characteristics based on both categorization schemes. Category collisions such as CWB 1 with NEHRP D as well as CWB 3 with NEHRP B occur, pointing out the futility of either modeling such data as well as using it in empirical regressions, until the sites are classified using a useful and reliable categorization scheme, with accompanying generic profiles. The adopted California based soft rock and deep soil profiles are shown in Figure 1.

3.2 Kocaeli And Duzce, Turkey Earthquakes

For the Turkey earthquakes many of the recording sites had shallow measured shear-wave velocity profiles (SASW; Professor Rathje, personal communication), greatly facilitating site classification and the development of realistic generic profiles to basement depths. The measured profiles generally fell into soft rock and deep firm soils, very similar to Northern California surficial geology based profiles for Franciscan (Fr) rock and Quaternary alluvium (Q_{al}) (Silva et al., 1998). As a result, the Northern California Franciscan and Quaternary alluvium generic profiles were adopted to model the geotechnical layer for the Turkey earthquakes recording sites. The shallow profiles (Figure 2) were placed on top of the regional crustal model (Table 1).

For both the Taiwan and Turkey sites, Northern California nonlinear dynamic material properties (Silva et al., 1998; EPRI, 1993) were assumed. Final assessment of the most appropriate G/G_{max} and hysteretic damping curves requires refinement of source parameters (slip model and rise time) and better characterization of the Chi-Chi, Taiwan earthquake site profiles.

Slip models and nucleation points used for all three earthquakes were taken from Somerville (personal communication). The slip models are shown in Figure 3 and were developed using inversions which accommodate both spatially varying rise times as well as rupture velocities. Since the stochastic finite fault model implemented here uses a fixed rise time and rupture velocity as well as a simpler approach to wave propagation, some inconsistencies likely exist between these slip models and ones optimized for the stochastic model. An inversion program was developed to determine optimum slip models, rupture velocity, and rise times but insufficient time was available to provide appropriate parameter constraints and thoroughly test the algorithm.

4. MODELING RESULTS

The results of the modeling are presented in a form that quantitatively measures how well the estimated 5% damped response spectra fit the average horizontal component spectra computed from the recorded motions. Two measures of "goodness of fit" are computed: the model bias, or average misfit over all sites at each frequency and the uncertainty, a Chi-Square measure of fit over all sites at each frequency (Abrahamson et al., 1990). The average misfit or bias measures whether the model tends to over (negative bias) or under predict motions, for an average site. The uncertainty measures the site-to-site degree of misfit, giving information on how well the model accommodates the site-to-site variability in the recorded motions.

4.1 Chi-Chi, Taiwan Earthquake

For the **M** 7.6 Chi-Chi, Taiwan earthquake, Figure 4 shows the estimated model bias and uncertainty computed for 139 sites located within 50 km of the rupture surface using base case parameters (Table 6). For periods shorter than about 5-6 sec, the bias shows a large overprediction increasing with decreasing period and close to a factor of five at peak acceleration (100 Hz). A similar trend was seen by Boore (2001) in comparisons of Chi-Chi earthquake recordings with empirical attenuation relations based largely on California recordings.

These differences are consistent and suggest they are not due simply to earthquake-to-earthquake variability. Naturally, inappropriate shallow profiles as well as kappa values (Table 1) and dynamic material nonlinear properties (Figure 1) may contribute to this overprediction, particularly if typical soil sites are much shallower then the assumed 1,000 ft and stiffer as well. Additionally, generic rock sites in Taiwan may not have such a steep shallow gradient as typical California rock (Figure 1), which would result in much less amplification.

Apparently the Chi-Chi earthquake has significantly lower motions at periods less than several seconds than typical WNA (Western North America) earthquakes, which have been used to develop the finite fault base case parameters (Table 6). Because of the large bias, Figure 4a, the site-to-site variability shown in Figure 4b is extremely large, being dominated by the overprediction. The bias corrected uncertainty shows typical values (0.5 to 0.75) for uncorrected uncertainties based on modeling about 17 earthquakes at about 500 sites (Silva et al., 1997). Apart from the very unusual overprediction, the model captures site-to-site variability for this earthquake as well as the other validation earthquakes, or, put another way, the Chi-Chi earthquake does not appear to have an unusual degree of site-to-site variability, at least for distances out to 50 km.

To look at closer sites, Figure 5 shows results for all sites located within a 20 km rupture distance. In this case, the overprediction is reduced significantly for periods shorter than about 1 second to a value near 3 at peak acceleration. The reason for this is unclear but the same trend is seen in the comparisons of the Chi-Chi earthquake motions to WNA empirical predictions (Boore, 2001), the degree of overprediction decreases at larger distances. Without more and better site information it is difficult to assess whether this may be a site effect (more or fewer rock or soil sites at larger distances) or a wave propagation (crustal structure, Q(f), kappa) effect.

For comparison, Figure 5 also shows results computed using a subevent stress drop of 5 bars rather than the base case value of 30 bars. For this case the bias is near zero from 0.01 to about 20 seconds and the uncorrected uncertainty ranges from 0.5 to about 0.75. This suggests the overprediction of the Chi-Chi earthquake motions is related to source processes, particularly since increasing the rise time would have a similar effect. The average slip velocity for this earthquake may be lower than one would expect for a large reverse mechanism earthquake, based on California earthquakes.

4.2 Turkey Earthquakes

Figure 6 shows the model bias and uncertainty computed for the Kocaeli, Turkey earthquake at all 34 sites, rupture distances out to over 400 km (Table 4). The bias is near zero but shows an underprediction at long periods, exceeding about 3 seconds. There is some evidence of rupture velocities exceeding shear-wave velocities for this earthquake, reaching some 4.5 km/sec, near the limit of $\sqrt{2}$ times the shear-wave velocity (3.5 km/sec, Table 1) for stable rupture

propagation (Bouchon et al., 2001). Increasing the rupture velocity over the base case value of 2.8 km/sec (Table 6) would enhance the long period motions.

The uncertainty (Figure 6b) computed over all the sites is higher than typical (Silva et al., 1997), ranging from about 0.75 at peak acceleration to about 1 at 10 seconds. Examining the closer sites (within a 50 km rupture distance) reveals a general overprediction at periods shorter than about 3 seconds (Figure 7). Apart from the bias, the uncertainty shown in Figure 7b has reduced (bias corrected) suggesting less site-to-site variability for the closer sites. As with the Chi-Chi earthquake, inversions for more appropriate slip models, rupture velocities, and rise times are required to resolve the over prediction for the sites within a 50 km rupture distance.

For the Duzce earthquake, Figures 8 and 9 show similar results as the Kocaeli earthquake. In this case however, a significant overprediction exists over all 22 sites (Figure 8a) and the overprediction for sites within a 50 km rupture distance is extreme (Figure 9a). To a large extent this may be driven by a few sites very near the rupture which recorded extremely low short period motions. For example, sites 058, 1059, 531, 1062, and 1061 at rupture distances of 1, 8, 11, 13, and 16 km respectively (Table 5) have average peak accelerations of less than 20%g. This is very unusual, even for a normal mechansim and significantly more study is required to resolve this issue, as well as the overpredictions of the Kocaeli and Chi-Chi earthquakes.

The general procedure followed when the model was last validated using a large suite of earthquakes (15, Silva et al., 1997) was to find the best fitting rupture velocities, rise times, and subevent stress drop as well as Q(f) models, small strain kappa values, and nonlinear dynamic material properties (Silva et al., 1998). Q(f) and kappa models are first estimated using point-source inversions (for stress drop, Q(f), and kappa values). The Q(f) and small stress initial kappa models are then used in finite fault simulations where rise time, rupture velocity, and subevent stress drop are varied for each earthquake to minimize the bias. Average values over all earthquakes are then estimated (a rise time verses moment relation developed) and the validations redone with the "global" average values for rupture velocity, rise time, and subevent stress drop. This approach results in a larger uncertainty over all earthquakes but eliminates the need for developing and defending parametric distributions for these parameters for the next earthquake. This process should be repeated (updated) as new earthquakes are added to the validation set. Once reliable site conditions and generic profiles are available for the Chi-Chi, Taiwan earthquake and it is considered to be representative of California earthquakes and the near source sites for the Duzce, Turkey earthquake are judged to be useable, this update process will be implemented for the stochastic finite source model.

5. REFERENCES

Abrahamson, N.A. and Silva, W.J. (1997). "Empirical response spectral attenuation relations for shallow crustal earthquakes." *Seism. Res. Lett.*, 68(1), 94-127.

Abrahamson, N.A., Somerville, P.G., Cornell, C.A. (1990). "Uncertainty in numerical strong motion predictions" *Proc. Fourth U.S. Nat. Conf. Earth. Engin.*, Palm Springs, CA., 1, 407-416.

Bouchon, M., M-P. Boui, H. Karabulut, M. N. Toksoz, M. Dietrich, and A. J. Rosakis (2001). "How fast is rupture during an earthquake? New insights from the 1999 Turkey earthquakes." *Geophys. Res. Let.,* 28(14) 2723-2726.

Boore, D. M. (2001). "Comparisons of ground motions from the 1999 Chi-Chi earthquake with empirical predictions largely based on data from California." *Bull. Seism. Soc. Am.,* 91(5), 1212-1217.

Electric Power Research Institute (1993). "Guidelines for determining design basis ground motions." Palo Alto, Calif: Electric Power Research Institute, vol. 1-5, EPRI TR-102293. vol. 1: Methodology and guidelines for estimating earthquake ground motion in eastern North America.

vol. 2: Appendices for ground motion estimation.
vol. 3: Appendices for field investigations.
vol. 4: Appendices for laboratory investigations.
vol. 5: Quantification of seismic source effects.

Lee, C.-T., C.-T., Cheng, C.-W., Liao, and Y.-B., Tsai (2001). "Site classification of Taiwan free-field strong-motion stations". *Bull. Seism. Soc. Am.*, 91(5), 1283-1297.

Neugebauer, J., M. Loeffler, H. Berckhemer, and A. Yatman (1997). "Seismic observations at an overstep of the western North Anatolian Fault (Abant-Sapanca region, Turkey). *Geol. Rundsch.*, 86, 93-102.

Roecker, S.W., Y. H. Yeh, and Y. B. Tsai (1987). "Three-dimensional P and S wave velocity structures beneath Taiwan: Deep structure beneath an ARC-Continent collision". *J. of Geoph. Research*, 92(B10), 10,547-10,570.

Sadigh, C.-Y. Chang, J.A. Egan, F. Makdisi, and R.R. Youngs (1997). "Attenuation relationships for shallow crustal earthquakes based on California strong motion data." *Seism. Soc. Am.*, 68(1), 180-189.

Silva, W.J. Costantino, C. Li, Sylvia (1998). AQuantification of nonlinear soil response for the Loma Prieta, Northridge, and Imperial Valley California earthquakes.@ *The effects of Surface Geology on Seismic Motion*, Irikura, Kudo, Okada & Sasatani (eds.).

Silva, W.J., N. Abrahamson, G. Toro and C. Costantino. (1997). "Description and validation of the stochastic ground motion model." Report Submitted to Brookhaven National Laboratory, Associated Universities, Inc. Upton, New York 11973, Contract No. 770573.

Sokolov, V. Y., C.-H. Loh, K.-L. Wen (2001). "Empirical models for site- and region-dependent ground-motion parameters in the Taipei Area: A unified approach" *Earthquake Spectra,* 17(2), 313-333.

Table 1 CRUSTAL MODELS		
Chi-Chi, Taiwan*		
Th (km)	V_S (km/sec)	ρ (cgs)
1.5**	1.98	2.30
9.0	3.35	2.60
8.0	3.52	2.80
19.0	3.87	2.87
	4.50	3.20
$Q(f) = 125\ f^{0.8}$ (Sokolov et al., 2001) $\kappa = 0.04$ sec***		
Koaceli, Duzce, Turkey****		
0.5	1.00	2.00
1.5	1.60	2.10
5.0	3.00	2.50
10.0	3.50	2.78
18.0	3.70	2.90
	4.60	3.40
$Q(f) = 180\ f^{0.6}$ (Silva et al., 1997; generic California assumed) $\kappa = 0.04$ sec***		

*Roecher et al. (1987)

**Surficial firm rock layer added

***Small strain kappa set to 0.04 sec at both rock and soil sites (Silva et al., 1997).

****Neugebauer et al. (1997)

Table 2 CHI-CHI EARTHQUAKE SITES			
Station	Rupture Distance (km)	CWB Site Class	NEHRP Site Class
TCU052	.09	1	c*
CHY080	.39		B
TCU067	.89	1	C
TCU068	1.06	1	C
TCU087	1.25	1	b*
TCU102	2.30	2	C
TCU129	2.43	2	C
WNT	2.43	1	C
TCU103	3.40	1	c*
TCU101	3.43	2	C
TCU065	3.49	1	C
TCU076	3.59	2	C
TCU071	3.76	1	C
TCU075	4.11	2	C
TCU049	4.74	2	C
TCU	5.87	2	C
TCU082	5.87	2	C
TCU054	6.11		C
TCU053	7.00	2	C
TCU055	7.00		C
ALS	7.11	1	b*
TCU072	7.24	1	C
TCU078	7.74	1	C
TCU089	7.87	1	b*
NSY	7.97	2	B
TCU128	7.97	1	B
CHY028	8.08	1	C
TCU051	8.46		C
CHY024	9.18	1	C
CHY035	9.19	1	C
TCU122	9.41		C
TCU136	9.53		B
TCU060	9.90	2	C
TCU079	10.23	1	C
TCU084	10.31	1	B
TCU050	10.60	2	C
TCU120	10.67	1	B
TCU056	11.30	1	D

Table 2 (cont.) CHI-CHI EARTHQUAKE SITES			
Station	Rupture Distance (km)	CWB Site Class	NEHRP Site Class
TCU063	11.65	2	C
CHY041	11.83	1	D
TCU138	11.94		C
TCU116	12.81	3	D
TCU057	12.83		B
TCU036	12.89	1	C
CHY101	13.00	2	C
WGK	13.00	2	C
CHY034	13.21	1	C
TCU074	13.25	2	C
TCU104	14.03		B
CHY006	14.33	1	C
CHY010	14.48	1	C
TCU064	14.56	2	C
TCU048	14.66	1	B
TCU110	14.88	3	D
TCU046	15.38	1	A
CHY029	15.70	1	B
TCU109	15.95	1	C
TCU039	16.59	1	B
TCU040	16.75	2	D
TCU123	18.18	2	C
TCU106	18.19	2	C
TCU059	18.47		C
TCU105	18.61		B
TCU038	18.63	2	C
TCU061	18.66	2	C
CHY025	18.79	2	D
TCU070	19.44		B
CHY042	19.95	1	B
CHY086	20.25	1	B
CHY036	20.75	2	C
TCU107	20.96	2	C
CHY087	21.50	1	B
CHY027	21.82	3	D
CHY046	22.01	1	C
CHY092	22.56		D
CHY104	22.66	3	D
CHY047	23.30	1	C
TCU029	23.73	1	B
TCU042	23.75	2	C
TCU141	24.41		D
TCU045	24.43		B

Table 2 (cont.) CHI-CHI EARTHQUAKE SITES			
Station	Rupture Distance (Km)	CWB Site Class	NEHRP Site Class
TCU031	24.65	1	C*
TCU111	24.78	3	D
TCU115	25.05	3	D
CHY014	26.20	1	C
KAU054	26.34	1	b*
TCU117	27.68	3	D
CHY002	28.50		D
CHY026	29.42	3	D
TCU112	30.68	3	D
CHY102	30.80	1	B
CHY052	30.98	1	b*
CHY088	31.36	1	C
CHY015	32.84	3	C
TCU113	32.89	1	D
CHY109	32.98		b*
CHY110	32.98		b*
TCU047	33.17		B
TCU034	33.69	1	B
CHY039	33.70	2	D
CHY081	33.71	1	B
NST	35.87	1	C
TCU140	36.27		D
HWA053	36.51		A
ILA067	36.97		B**
HWA024	37.42	2	B
HWA038	37.88	2	B
HWA054	37.97		C
TCU145	38.38		D
CHY094	38.47	3	D
TCU033	38.88	1	C
TTN051	38.91		B**
CHY032	39.24	3	D
HWA036	39.24	2	C
HWA034	39.41	2	C
HWA039	39.97	2	C
CHY082	40.10	3	D
TCU119	40.77		D
HWA055	41.05		C
HWA037	41.10		C
HWA032	41.45		C
CHY008	41.51	2	D
HWA005	41.86	2	C
HWA006	42.03	2	C

Table 2 (cont.) CHI-CHI EARTHQUAKE SITES			
Station	Rupture Distance (Km)	CWB Site Class	NEHRP Site Class
ESL	42.21	1	C
HWA020	42.21	1	C
TCU095	42.43	1	B
WTC	43.30	3	D
HWA030	43.76	2	C
HWA035	43.82	2	C
HWA056	45.54		A
TCU098	45.66	1	C
HWA058	45.92		B**
HWA033	46.65	2	B
CHY033	46.86	3	D
CHY076	47.17	3	D
WSF	47.17	1	D
TCU015	47.78	1	B

** ASSUMED SITE CONDITION

NEHRP site codes for the Chi-Chi, Taiwan earthquake are from the paper by Lee et al. (2001). These were taken as the suggested NEHRP site classification. Questionable site classification stations are indicated with a lower case letter and an "*" in the next column.

Central Weather Bureau (CWB) of Taiwan Site Categories

1 = Hard site.
2 = Medium site.
3 = Soft soil site.

NEHRP 1-LETTER SITE CLASSIFICATIONS

Average shear-wave velocity to a depth of 30m is:
A > 1500 m/s
B = 750 - 1500 m/s
C = 360 - 750 m/s
D = 180 - 360 m/s
E = < 180 m/s
Lower case letter indicates a questionable site classification for the Chi-Chi, Taiwan earthquake stations.

Table 3 CHI-CHI EARTHQUAKE SITE CATEGORY MAPPING		
NEHRP	CWB Site Class	GEOMATRIX* Site Class
A		AB
A	1	AB
A	2	AB
A	3	
B		
B	1	AB
B	2	AB
B	3	
C		AB
C	1	AB
C	2	CD
C	3	CD
D		CD
D	1	AB
D	2	CD
D	3	CD

*Geomatrix AB = soft rock, CD = deep firm soil

Table 4 KOCAELI EARTHQUAKE SITES		
Station	Rupture Distance (Km)	Geomatrix Site Class
SKR	2.57	B
YPT	5.53	D
IZT	5.81	A
GBZ	8.01	A
ARC	12.16	B
DZC	15.35	D
IZN	30.26	D
ATK	30.53	D
GYN	36.54	B
ZYT	45.56	D
FAT	45.67	C
IST	45.78	B
MCD	47.18	B
YKP	48.03	A
MSK	49.87	A
DHM	51.13	D
BUR	54.42	D
CNA	57.97	D
CEK	59.00	D*
ATS	59.26	D
BRS	60.92	A
BTS	116.72	D
ERG	131.94	D*
KUT	143.80	D
TKR	154.65	A
BLK	170.50	D
AFY	213.63	D*
USK	226.73	D*
TOS	251.57	D*
CNK	254.11	D*
MNS	284.41	D*
BRN	306.40	D*
AYD	342.83	D*
TKT	413.15	B*

*ASSUMED SITE CONDITION

Site categories for the Turkey earthquakes are from Prof. E. Rathje, University of Texas at Austin.

GEOMATRIX SITE CLASSIFICATION

A = Rock. Instrument on rock (Vs > 600 mps) or < 5m of soil over rock.

B = Shallow (stiff) soil. Instrument on/in soil profile up to 20m thick overlying rock.

C = Deep narrow soil. Instrument on/in soil profile at least 20m thick overlying rock, in a narrow canyon or valley no more than several km wide.

D = Deep broad soil. Instrument on/in soil profile at least 20m thick overlying rock, in a broad valley.

E = Soft deep soil. Instrument on/in deep soil profile with average Vs < 150 mps.

A and B = Taken as Soft Rock

C and D = Taken as Deep Firm Soil

Table 5 DUZCE EARTHQUAKE SITES		
Station	Rupture Distance (Km)	Geomatrix Site Class
1058	0.9	B
375	8.2	B
DZC	8.2	D
1059	8.5	B
531	11.4	A
1062	13.3	B
1061	15.6	B
BOL	17.6	D
362	27.4	B
1060	30.2	A
MDR	36.6	A
SKR	49.9	B
YPT	101.7	D
DAR	134.9	D
ARC	135.7	B
BUR	169.3	D
KUT	169.5	D
FAT	172.5	C
KMP	174.0	C
DHM	182.7	B
CNA	188.4	B
ATS	193.3	D

Table 6 FINITE SOURCE MODEL PARMETERS			
	Chi-Chi	Kocaeli	Duzce
Magnitude	7.6	7.4	7.1
Rupture Length (km)	92.4	150.0	50.0
Rupture Width (km)	48.0	19.8	25.0
Dip (deg)	32.0	0.	70.0
Mechanism	R	S	N
Rise Time (sec)	3.3	2.6	1.9
Rupture Velocity (km/sec)	2.8	2.8	2.8
Subevent Stress Drop (bars)	30.0*	30.0	30.0

*5 bars also run

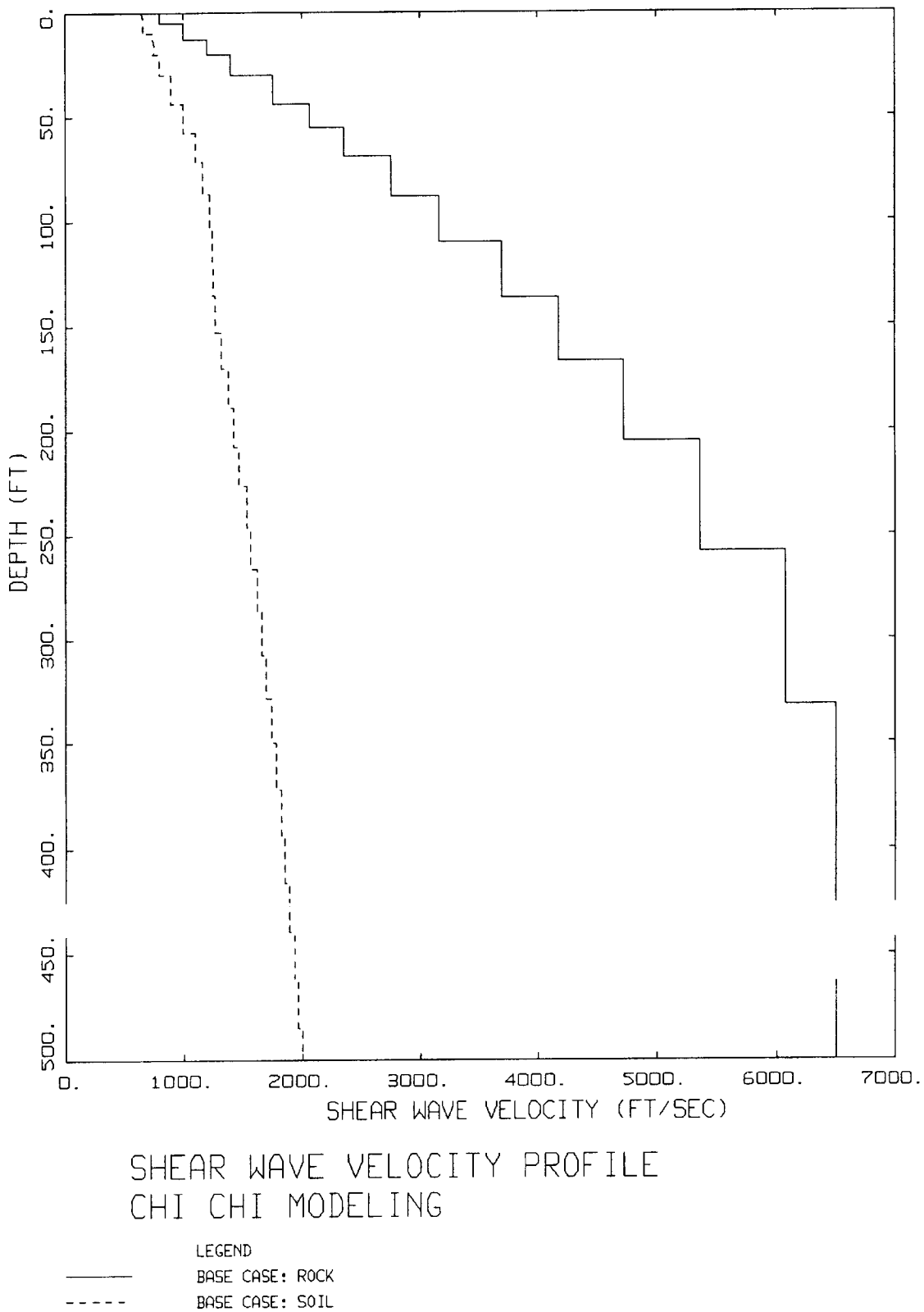

Figure 1. Shallow shear-wave velocity profiles used at rock and soil sites for the Chi-Chi, Taiwan earthquake. Profiles were placed on top of the regional crustal model (Table 1).

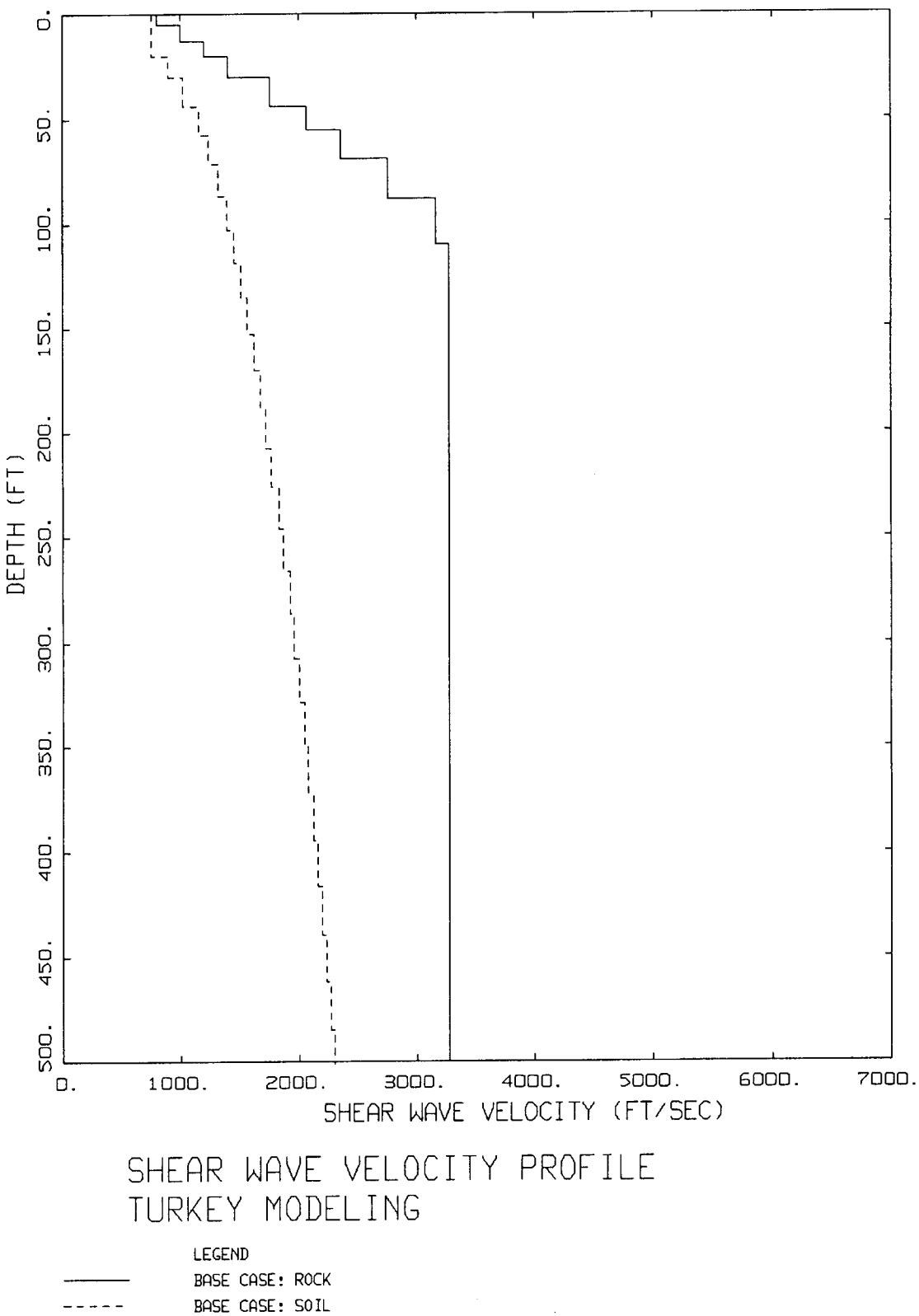

Figure 2. Shallow shear-wave velocity profiles used at rock and soil sites for the Kocaeli and Duzce, Turkey earthquake. Profiles were placed on top of the regional crustal model (Table 1).

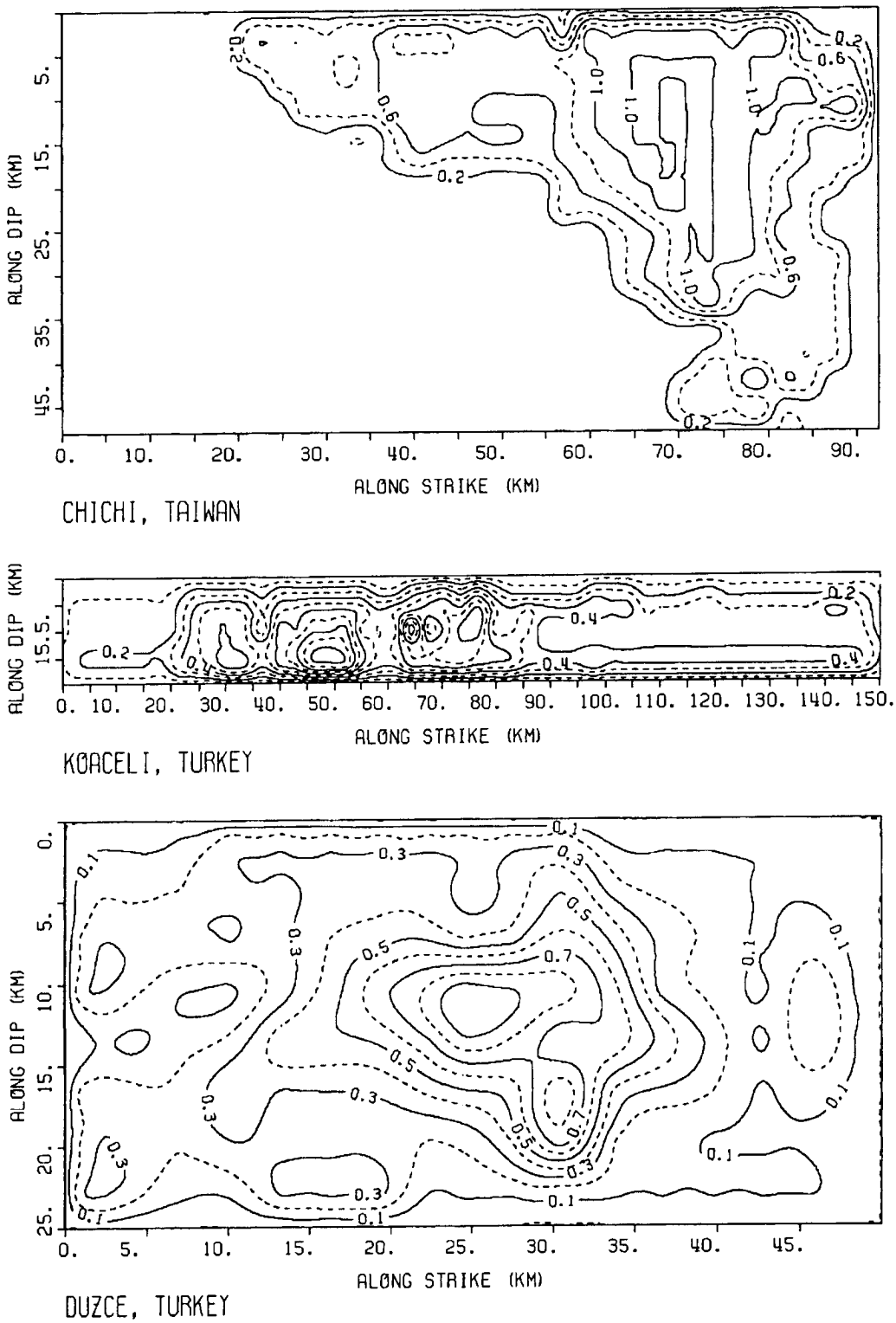

Figure 3. Relative slip models used for the Chi-Chi, Taiwan and Kocaeli and Duzce, Turkey earthquakes.

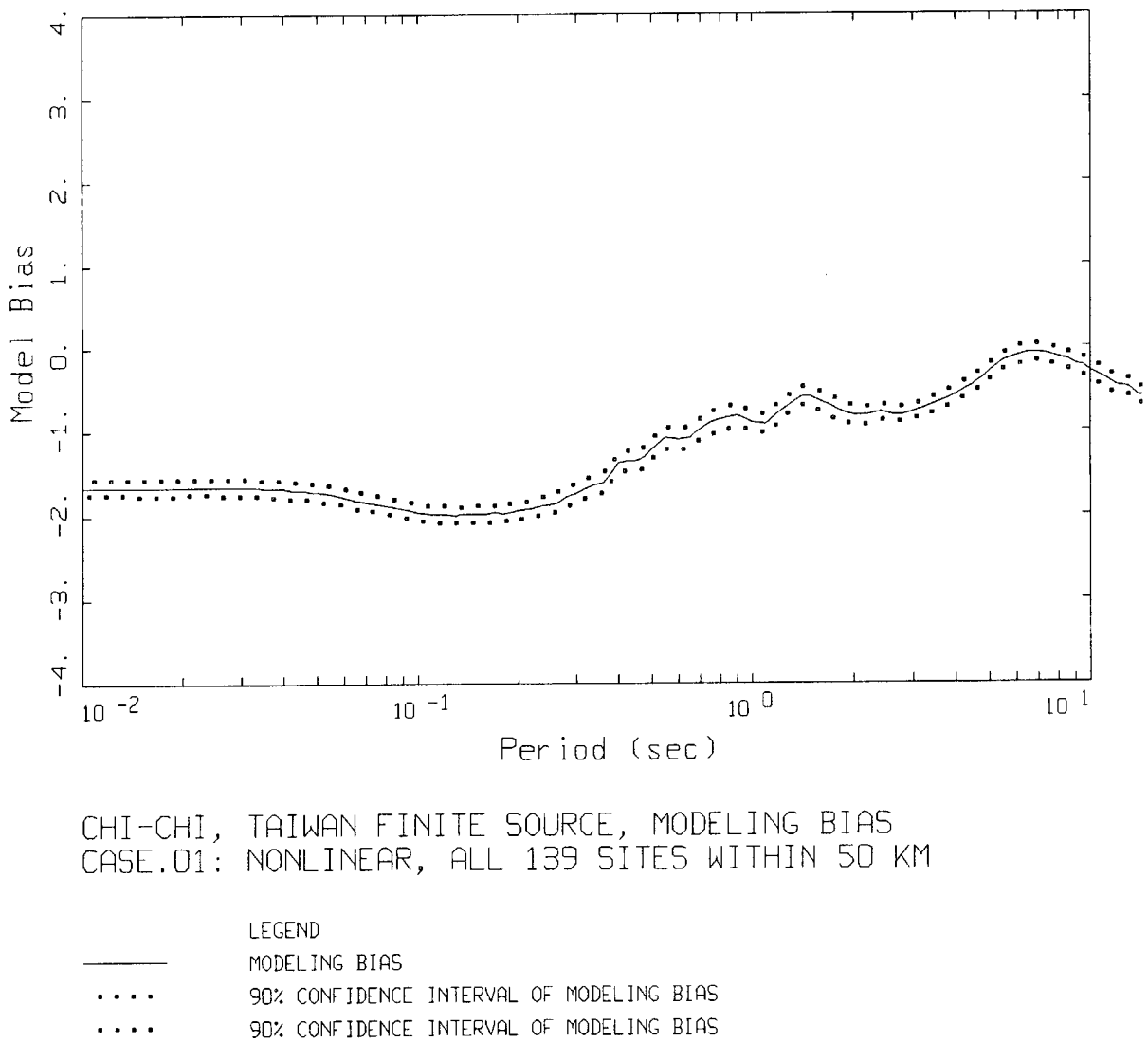

Figure 4a. Model bias computed for the Chi-Chi, Taiwan earthquake using base case parameters: all 139 sites within a 50 km rupture distance (Table 2).

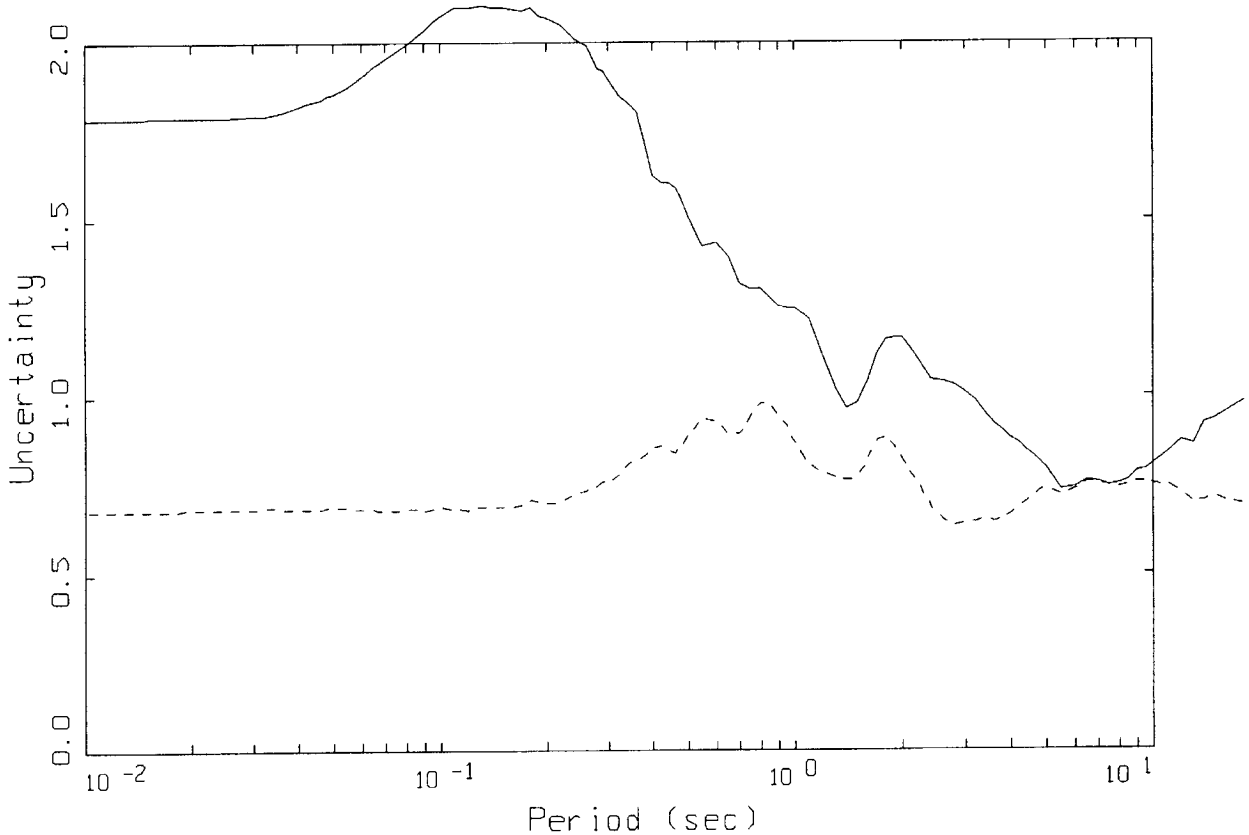

Figure 4b. Model variability computed for the Chi-Chi, Taiwan earthquake using base case parameters: all 139 sites within a 50 km rupture distance (Table 2).

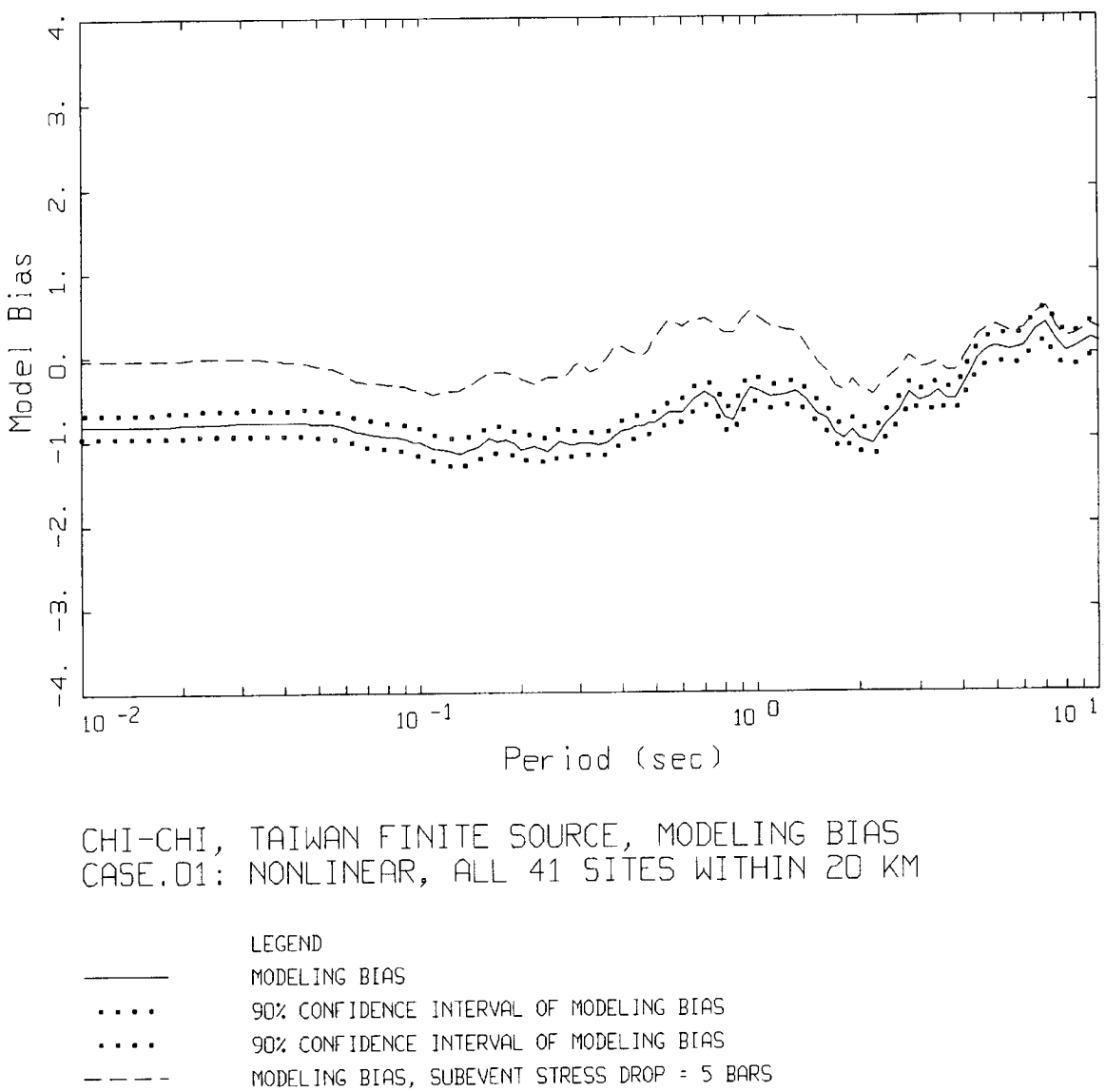

Figure 5a. Model bias computed for the Chi-Chi, Taiwan earthquake using base case parameters: all 41 sites within a 20 km rupture distance (Table 2). Results using a 5 bar subevent stress drop also shown.

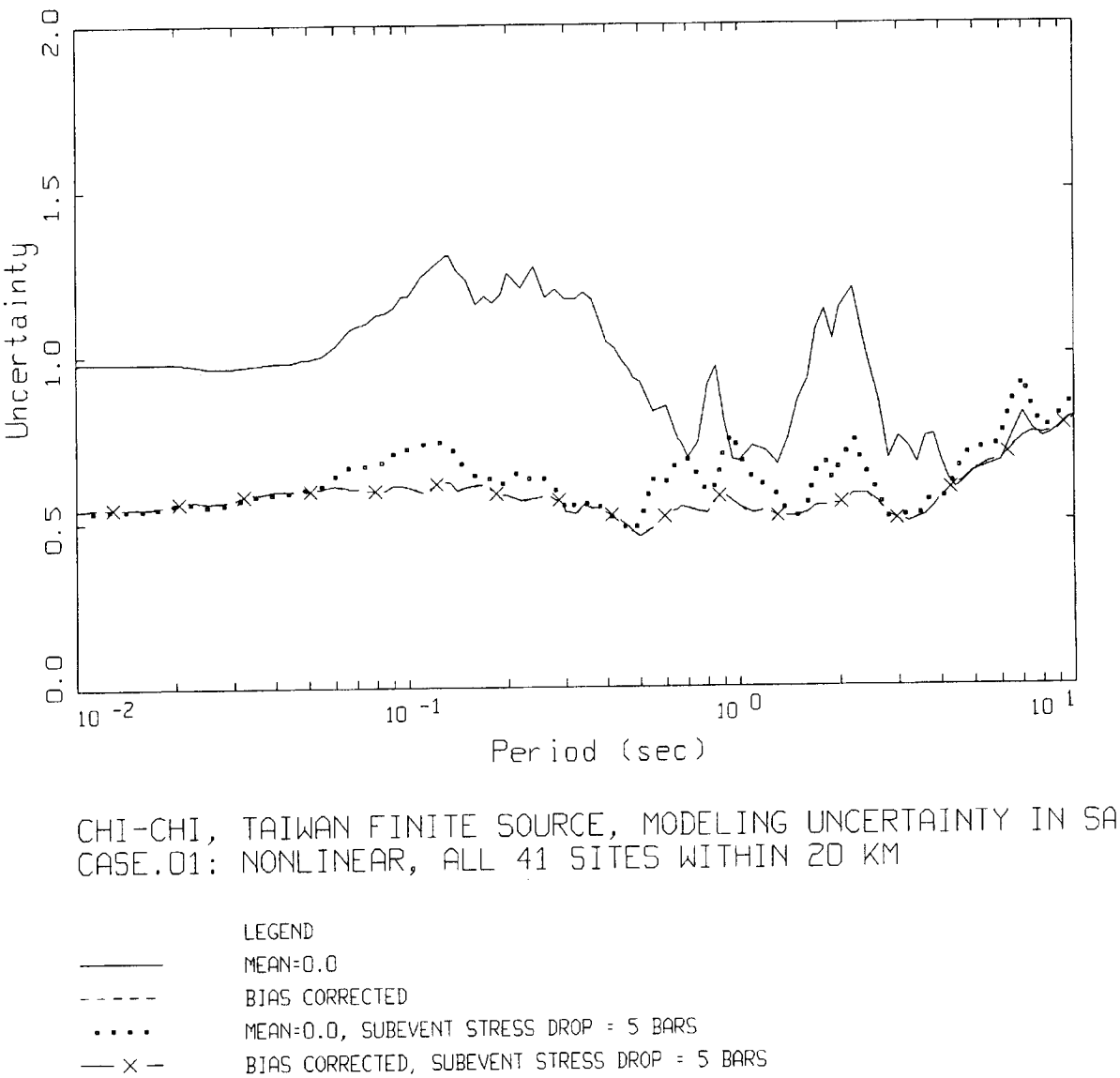

Figure 5b. Model bias computed for the Chi-Chi, Taiwan earthquake using base case parameters: all 41 sites within a 20 km rupture distance (Table 2). Results using a 5 bar subevent stress drop also shown.

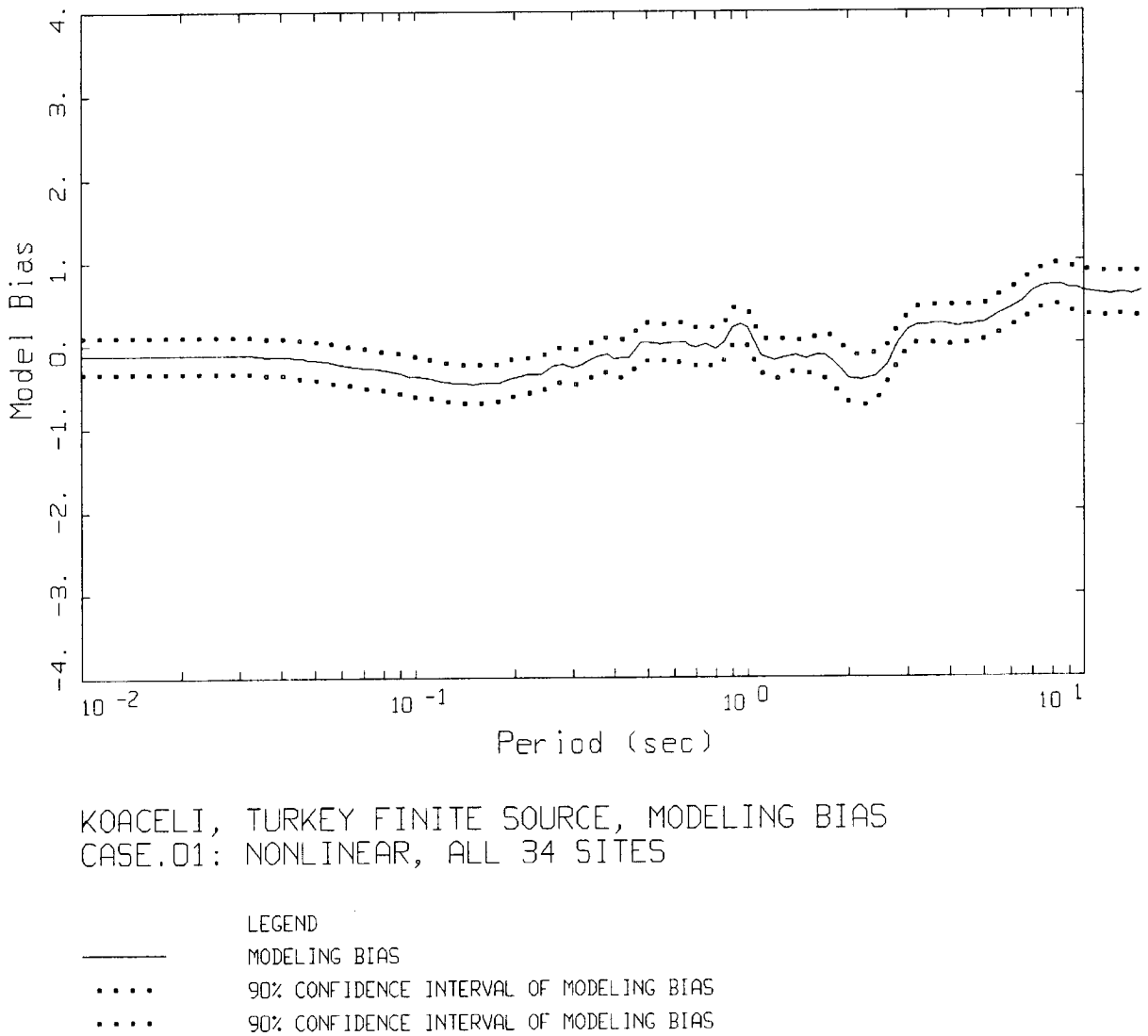

Figure 6a. Model bias computed for the Kocaeli, Turkey earthquake using base case parameters: all 34 sites (Table 4).

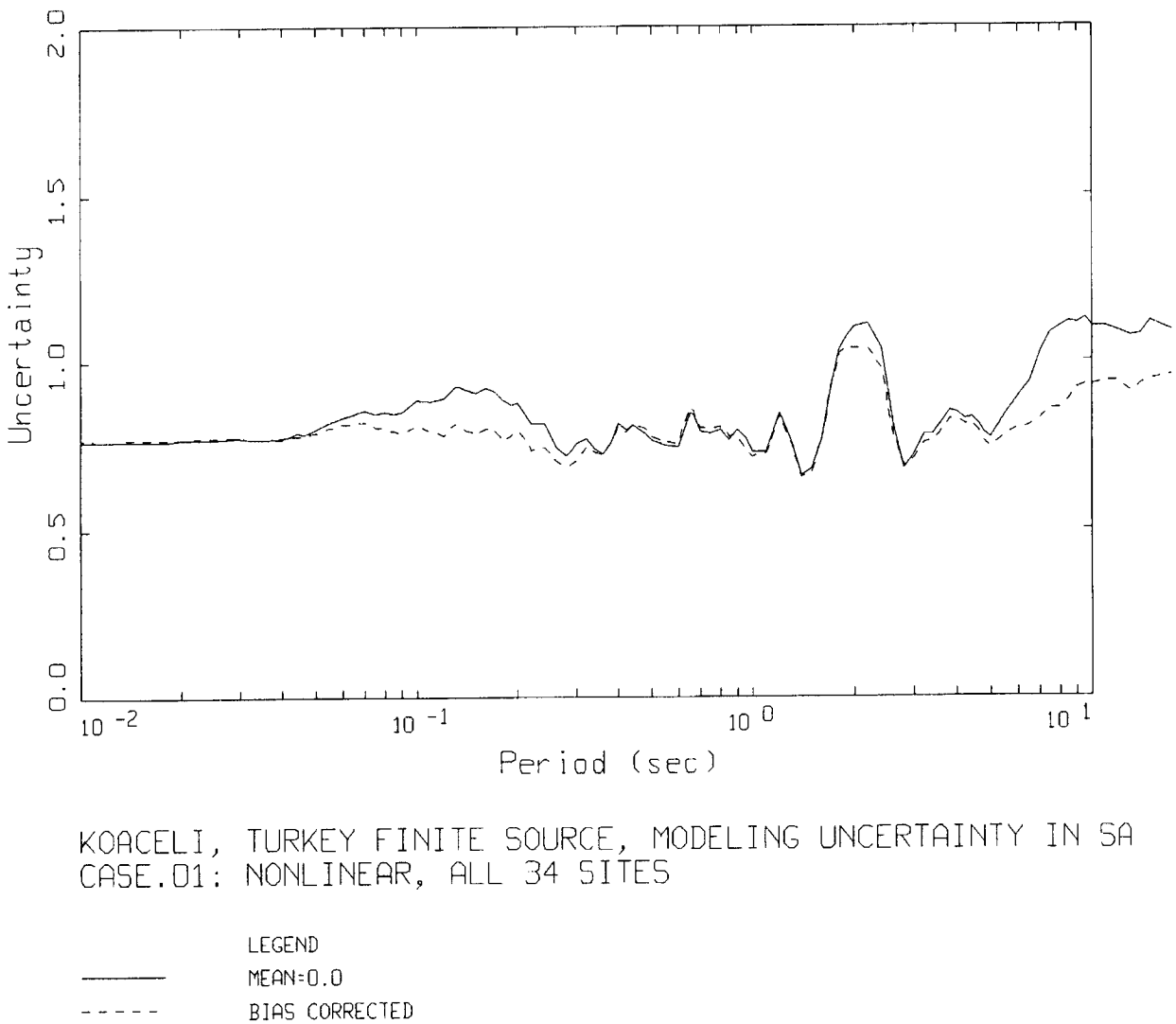

Figure 6b. Model variability computed for the Kocaeli, Turkey earthquake using base case parameters: all 34 sites (Table 4).

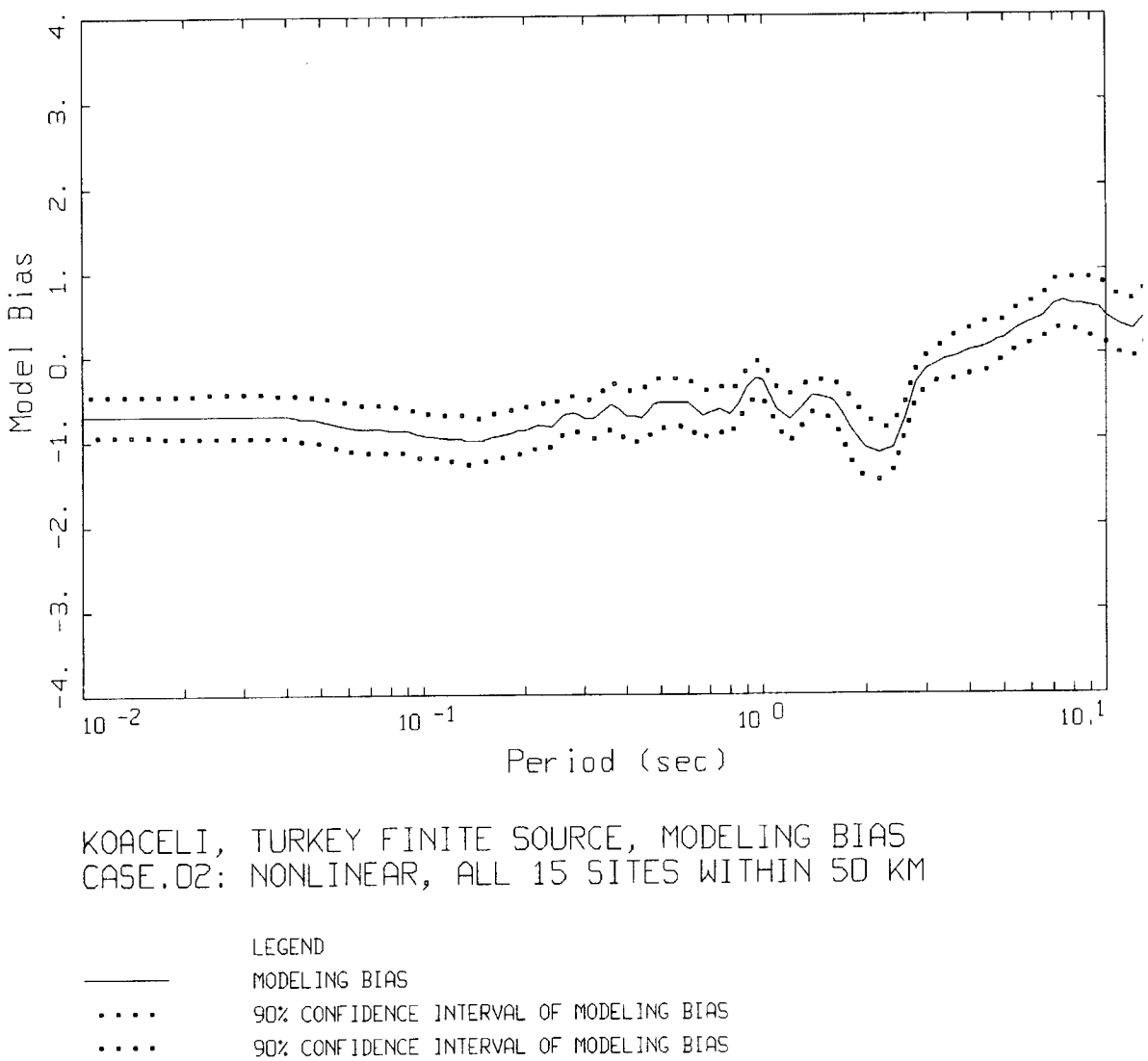

Figure 7a. Model bias computed for the Kocaeli, Turkey earthquake using base case parameters: all 15 sites within a 50 km rupture distance (Table 4).

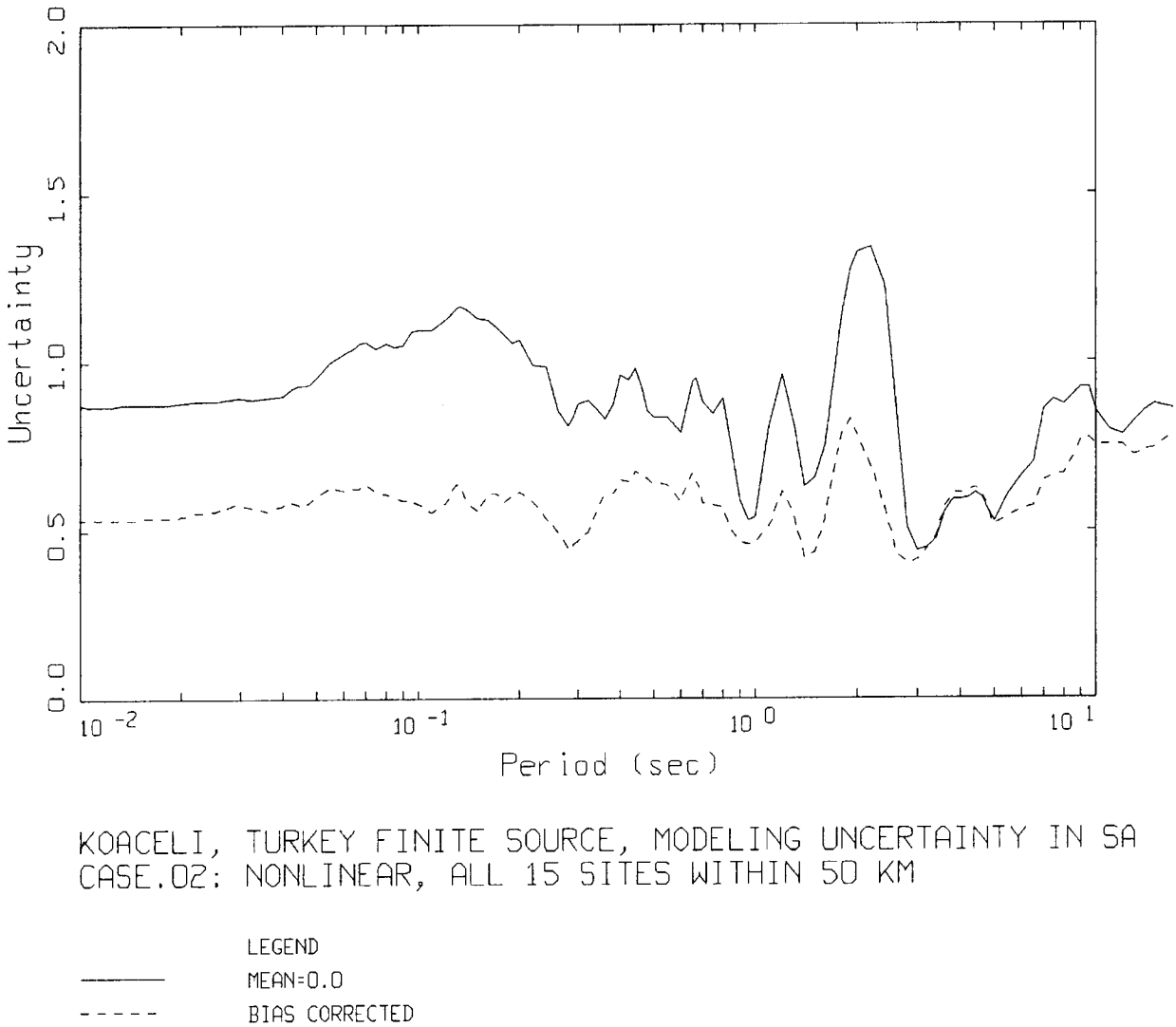

Figure 7b. Model variability computed for the Kocaeli, Turkey earthquake using base case parameters: all 15 sites within a 50 km rupture distance (Table 4).

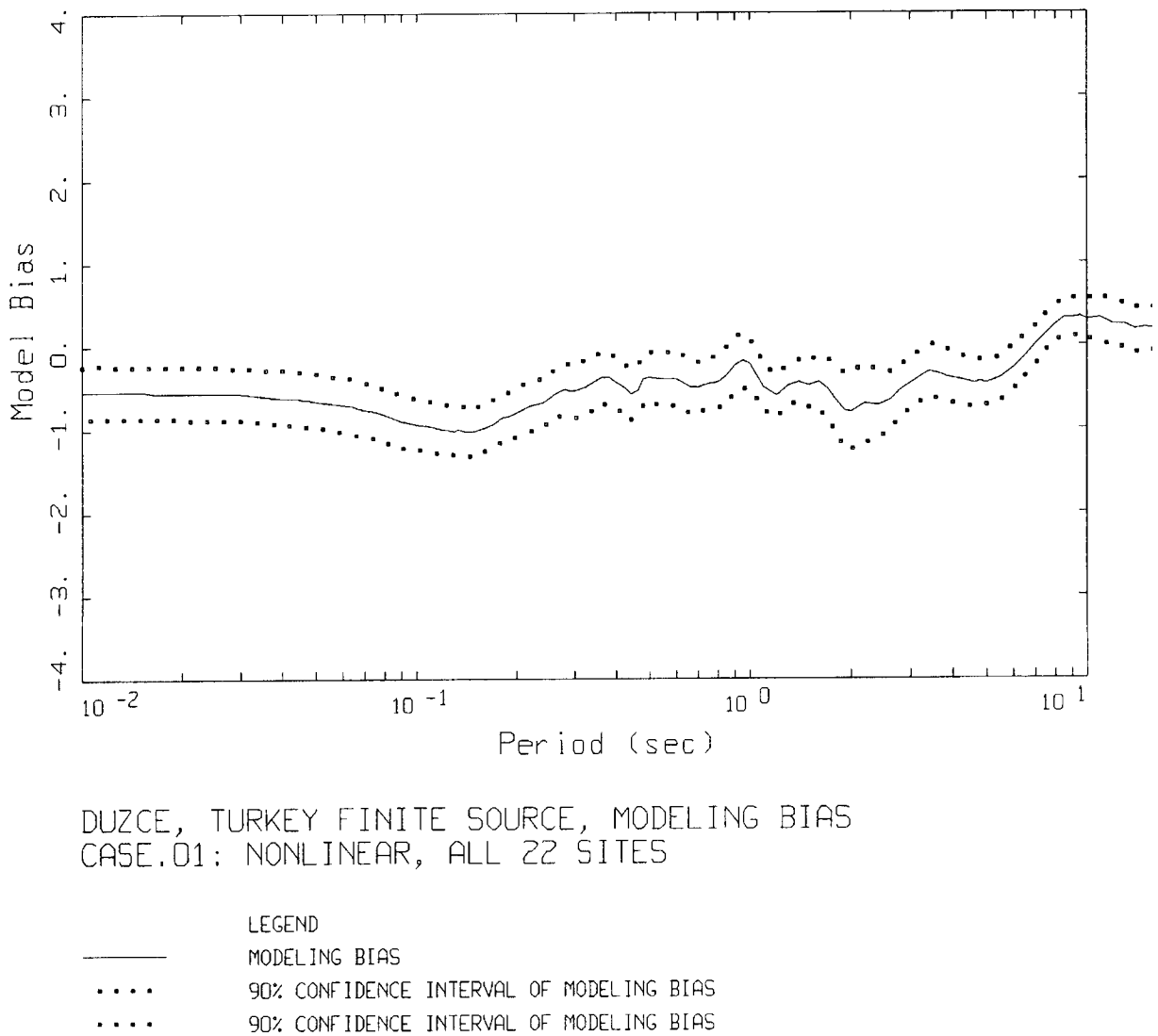

Figure 8a. Model bias computed for the Duzce, Turkey earthquake using base case parameters: all 22 sites (Table 5).

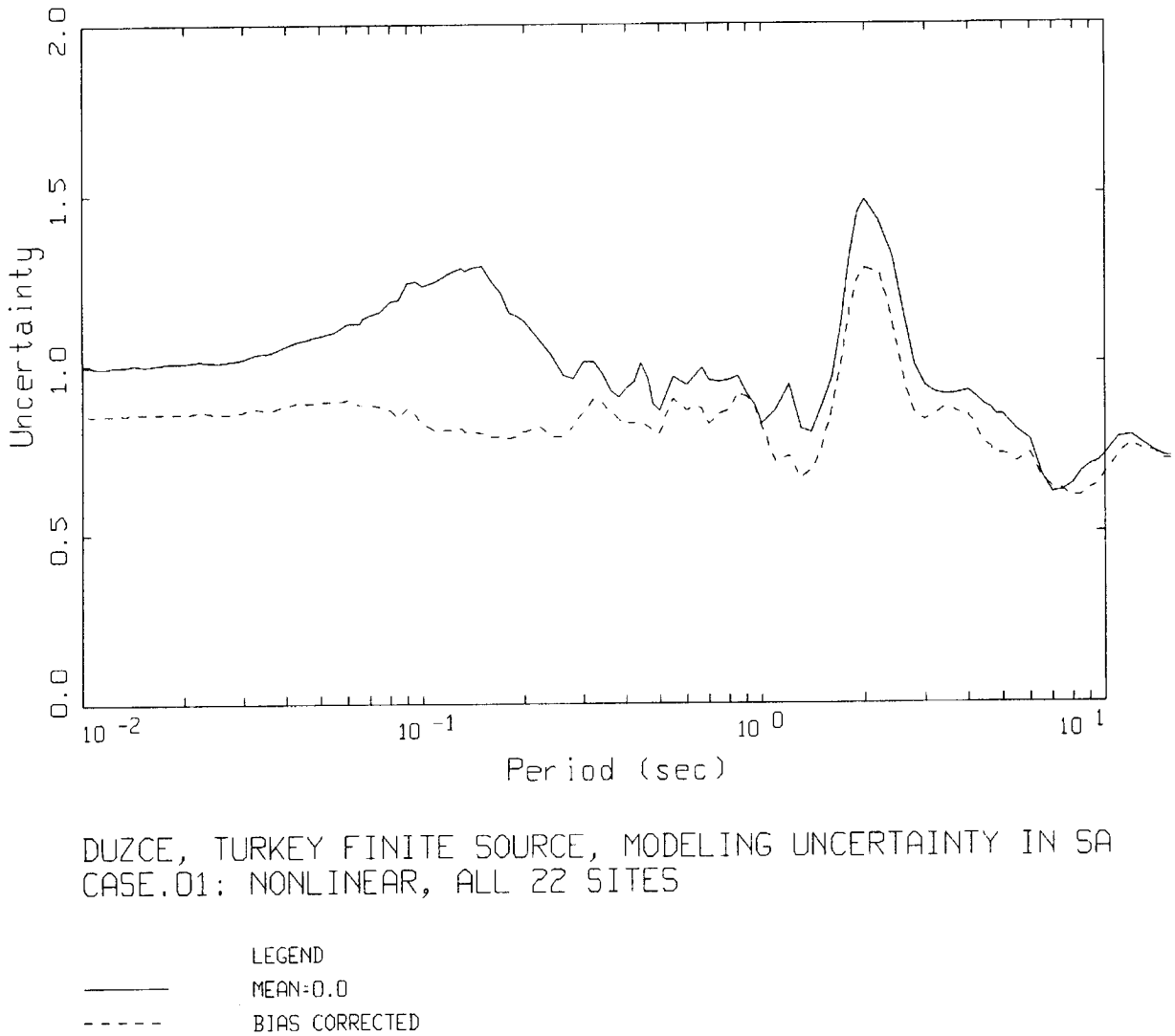

Figure 8b. Model variability computed for the Duzce, Turkey earthquake using base case parameters: all 22 sites (Table 5).

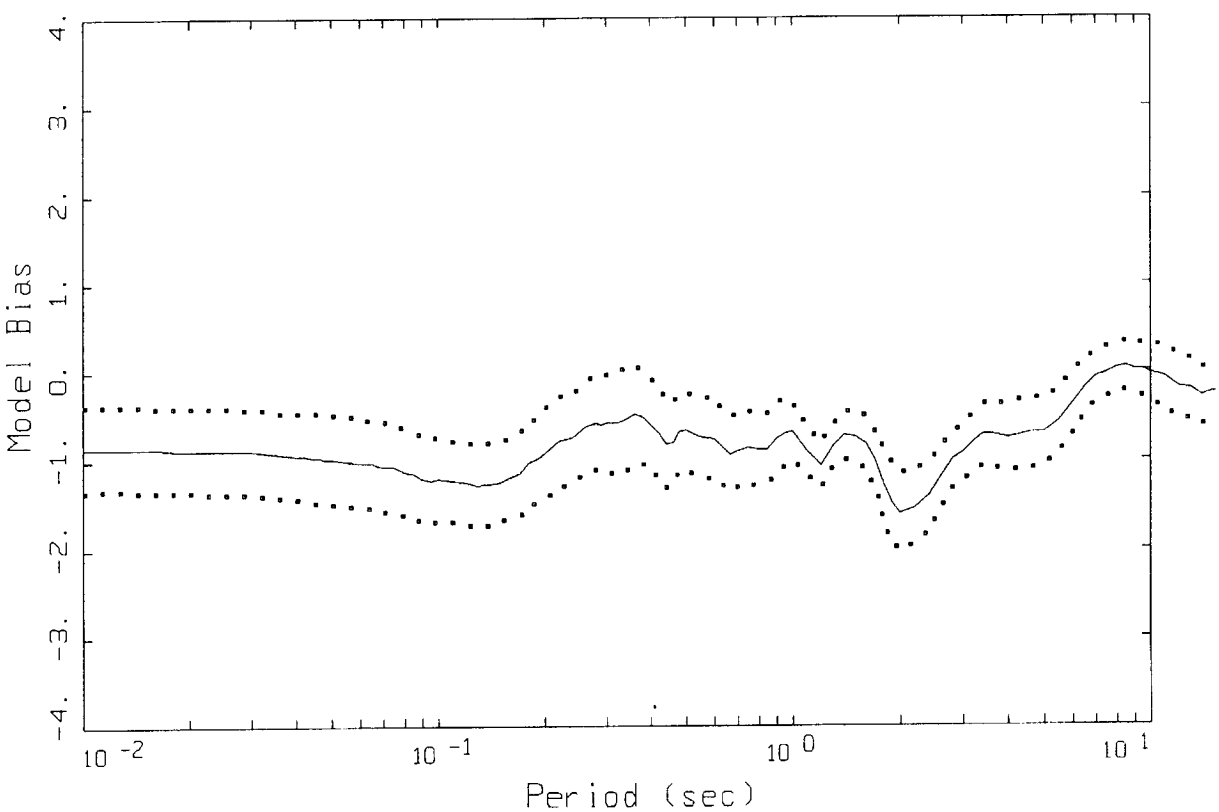

Figure 9a. Model bias computed for the Duzce, Turkey earthquake using base case parameters: all 12 sites within a 50 km rupture distance (Table 5).

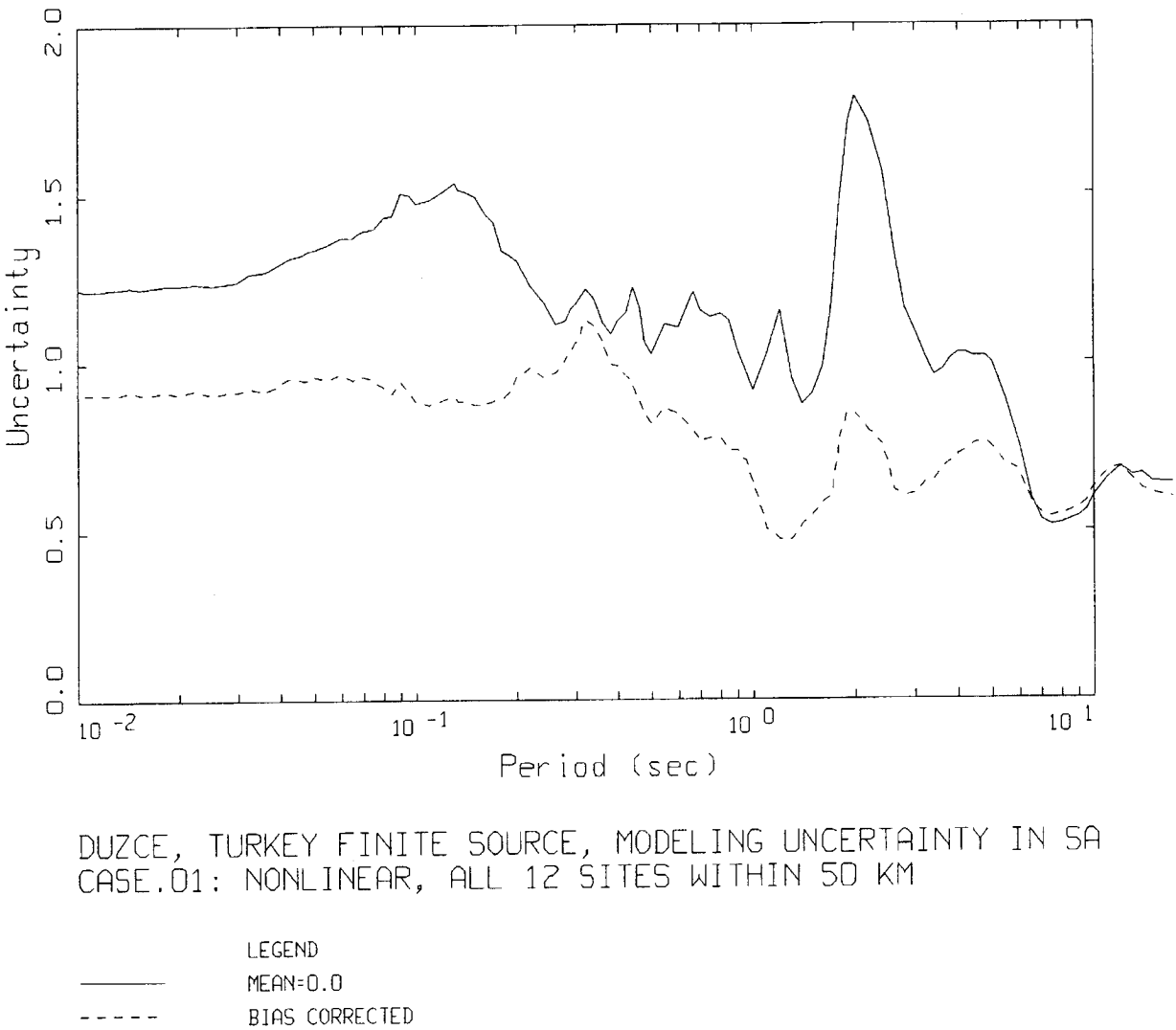

Figure 9b. Model variability computed for the Duzce, Turkey earthquake using base case parameters: all 12 sites within a 50 km rupture distance (Table 5).

APPENDIX A

STOCHASTIC GROUND MOTION MODEL DESCRIPTION

Background

In the context of strong ground motion, the term "stochastic" can be a fearful concept to some and may be interpreted to represent a fundamentally incorrect or inappropriate model (albeit the many examples demonstrating that it works well; Boore, 1983, 1986). To allay any initial misgivings, a brief discussion seems prudent to explain the term stochastic in the stochastic ground motion model.

The stochastic point-source model may be termed a spectral model in that it fundamentally describes the Fourier amplitude spectral density at the surface of a half-space (Hanks and McGuire, 1981). The model uses a Brune (1970, 1971) omega-square description of the earthquake source Fourier amplitude spectral density. This model is easily the most widely used and qualitatively validated source description available. Seismic sources ranging from **M** = -6 (hydrofracture) to **M** = 8 have been interpreted in terms of the Brune omega-square model in dozens of papers over the last 30 years. The general conclusion is that it provides a reasonable and consistent representation of crustal sources, particularly for tectonically active regions such as plate margins. A unique phase spectrum can be associated with the Brune source amplitude spectrum to produce a complex spectrum which can be propagated using either exact or approximate (1-2- or 3-D) wave propagation algorithms to produce single or multiple component time histories. In this context the model is not stochastic, it is decidedly deterministic and as exact and rigorous as one chooses. A two-dimensional array of such point-sources may be appropriately located on a fault surface (area) and fired with suitable delays to simulate rupture propagation on an extended rupture plane. As with the single point-source, any degree of rigor may be used in the wave propagation algorithm to produce multiple component or average horizontal component time histories. The result is a kinematic[1] finite-source model which has as its basis a source time history defined as a Brune pulse whose Fourier amplitude spectrum follows an omega-square model. This finite-fault model would be very similar to that used in published inversions for slip models if the 1-D propagation were treated using a reflectivity algorithm (Aki and Richards, 1980). This algorithm is a complete solution to the wave equation from static offsets (near-field terms) to an arbitrarily selected high frequency cutoff (generally 1-2 Hz).

Alternatively, to model the wave propagation more accurately, recordings of small earthquakes at the site of interest and with source locations distributed along the fault of interest may be used as empirical Green functions (Hartzell, 1978). To model the design earthquake, the empirical Green functions are delayed and summed in a manner to simulate rupture propagation (Hartzell, 1978). Provided a sufficient number of small

---

[1]Kinematic source model is one whose slip (displacement) is defined (imposed) while in a dynamic source model forces (stress) are defined (see Aki and Richards 1980 for a complete description).

earthquakes are recorded at the site of interest, the source locations adequately cover the expected rupture surface, and sufficient low frequency energy is present in the Green functions, this would be the most appropriate procedure to use if nonlinear site response is not an issue. With this approach the wave propagation is, in principle, exactly represented from each Green function source to the site. However, nonlinear site response is not treated unless Green function motions are recorded at a nearby rock outcrop with dynamic material properties similar to the rock underlying the soils at the site or recordings are made at depth within the site soil column. These motions may then be used as input to either total or effective stress site response codes to model nonlinear effects. Important issues associated with this approach include the availability of an appropriate nearby (1 to 2 km) rock outcrop and, for the downhole recordings, the necessity to remove all downgoing energy from the at-depth soil recordings. The downgoing energy must be removed from the downhole Green functions (recordings) prior to generating the control motions (summing) as only the upgoing wavefields are used as input to the nonlinear site response analyses. Removal of the downgoing energy from each recording requires multiple site response analyses which introduce uncertainty into the Green functions due to uncertainty i n dynamic material properties and the numerical site response model used to separate the upgoing and downgoing wavefields.

To alleviate these difficulties one can use recordings well distributed in azimuth at close distances to a small earthquake and correct the recordings back to the source by removing wave propagation effects using a simple approximation (say 1/R plus a constant for crustal amplification and radiation pattern), to obtain an empirical source function. This source function can be used to replace the Brune pulse to introduce some natural (although source, path, and site specific) variation into the dislocation time history. If this is coupled to an approximate wave propagation algorithm (asymptotic ray theory) which includes the direct rays and those which have undergone a single reflection, the result is the empirical source function method (EPRI, 1993). Combining the reflectivity propagation (which is generally limited to frequencies # 1-2 Hz due to computational demands) with the empirical source function approach (appropriate for frequencies $\exists$ 1 Hz; EPRI, 1993) results in a broad band simulation procedure which is strictly deterministic at low frequencies (where an analytical source function is used) and incorporates some natural variation at high frequencies through the use of an empirical source function (Sommerville et al., 1995).

All of these techniques are fundamentally similar, well founded in seismic source and wave propagation physics, and importantly, they are <u>all</u> approximate. Simply put, all models are wrong (approximate) and the single essential element in selecting a model is to incorporate the appropriate degree of rigor, commensurate with uncertainties and variabilities in crustal structure and site effects, through extensive validation exercises. It is generally felt that more complicated models produce more accurate results, however, the implications of more sophisticated models with the increased number of parameters which must be specified is often overlooked. This is not too serious a consequence in modeling past earthquakes since a reasonable range in parameter space can be explored to give the "best" results. However for future predictions, this increased rigor may carry undesirable baggage in increased parametric variability (Roblee et al., 1996). The effects of lack of knowledge (epistemic uncertainty; EPRI, 1993) regarding parameter values for

future occurrences results in uncertainty or variability in ground motion predictions. It may easily be the case that a very simple model, such as the point-source model can have comparable, or even smaller, total variability (modeling plus parametric) than a much more rigorous model with an increased number of parameters (EPRI, 1993). What is desired in a model is sufficient sophistication such that it captures the dominant and stable features of source, distance, and site dependencies observed in strong ground motions. It is these considerations which led to the development of the stochastic point- and finite-source models and, in part, leads to the stochastic element of the models.

The stochastic nature of the point- and finite-source RVT models is simply the assumption made about the character of ground motion time histories that permits stable estimates of peak parameters (e.g. acceleration, velocity, strain, stress, oscillator response) to be made without computing detailed time histories (Hanks and McGuire, 1981; Boore, 1983). This process uses random vibration theory to relate a time domain peak value to the time history root-mean-square (RMS) value (Boore, 1983). The assumption of the character of the time history for this process to strictly apply is that it be normally distributed random noise and stationary (its statistics do not change with time) over its duration. A visual examination of any time history quickly reveals that this is clearly not the case: time histories (acceleration, velocity, stress, strain, oscillator) start, build up, and then diminish with time. However poor the assumption of stationary Gaussian noise may appear, the net result is that the assumption is weak enough to permit the approach to work surprisingly well, as numerous comparisons with recorded motions and both qualitative and quantative validations have shown (Hanks and McGuire, 1981; Boore, 1983, 1986; McGuire et al., 1984; Boore and Atkinson, 1987; Silva and Lee, 1987; Toro and McGuire, 1987; Silva et al., 1990; EPRI, 1993; Schneider et al., 1993; Silva and Darragh, 1995; Silva et al., 1997). Corrections to RVT are available to accommodate different distributions as well as non-stationarity and are usually applied to the estimation of peak oscillator response in the calculated response spectra (Boore and Joyner, 1984; Toro, 1985).

Point-source Model

The conventional stochastic ground motion model uses an ω-square source model (Brune, 1970, 1971) with a single corner frequency and a constant stress drop (Boore, 1983; Atkinson, 1984). Random vibration theory is used to relate RMS (root-mean-square) values to peak values of acceleration (Boore, 1983), and oscillator response (Boore and Joyner, 1984; Toro, 1985; Silva and Lee, 1987) computed from the power spectra to expected peak time domain values (Boore, 1983).

The shape of the acceleration spectral density, a(f), is given by

$$a(f) = C \frac{f^2}{1+\left(\frac{f}{f_0}\right)^2} \frac{MSUB0}{R} P(f)\, A(f)\, e^{-\frac{\pi f R}{\beta_0 Q(f)}} \qquad \text{(A-1)}$$

where

$$C = \left(\frac{1}{\rho_0 \beta_0^3}\right) \bullet (2) \bullet (0.55) \bullet \left(\frac{1}{\sqrt{2}}\right) \bullet \pi.$$

M_0 = seismic moment,
R = hypocentral distance,
β_0 = shear-wave velocity at the source,
ρ_0 = density at the source
Q(f) = frequency dependent quality factor (crustal damping),
A(f) = crustal amplification,
P(f) = high-frequency truncation filter,
f_o = source corner frequency.

C is a constant which contains source region density (ρ_0) and shear-wave velocity terms and accounts for the free-surface effect (factor of 2), the source radiation pattern averaged over a sphere (0.55) (Boore, 1986), and the partition of energy into two horizontal components (1//2).

Source scaling is provided by specifying two independent parameters, the seismic moment (M_0) and the high-frequency stress parameter or stress drop ($\Delta\sigma$). The seismic moment is related to magnitude through the definition of moment magnitude **M** by the relation

$$\log M_0 = 1.5\,\mathbf{M} + 16.05 \qquad \text{(Hanks and Kanamori, 1979)} \qquad \text{(A - 2).}$$

The stress drop ($\Delta\sigma$) relates the corner frequency f_0 to M_0 through the relation

$$f_0 = \beta_0\,(\Delta\sigma/8.44\,M_0)^{1/3} \qquad \text{(Brune; 1970, 1971)} \qquad \text{(A - 3).}$$

The stress drop is sometimes referred to as the high frequency stress parameter (Boore, 1983) (or simply the stress parameter) since it directly scales the Fourier amplitude spectrum for frequencies above the corner frequency (Silva, 1991; Silva and Darragh 1995). High (> 1 Hz) frequency model predictions are then very sensitive to this parameter (Silva, 1991; EPRI, 1993) and the interpretation of it being a stress drop or simply a scaling parameter depends upon how well real earthquake sources (on average) obey the omega-square scaling (Equation A-3) and how well they are fit by the single-corner-frequency model (Atkinson and Silva, 1997). If earthquakes truly have single-corner-frequency omega-square sources, the stress drop in Equation A-3 is a physical parameter and its values have a physical interpretation of the forces (stresses) accelerating the relative slip across the rupture surface. High stress drop sources are due to a smaller source (fault) area (for the same **M**) than low stress drop sources (Brune, 1970). Otherwise, it simply a high frequency ($f > f_o$) scaling or fitting parameter.

The spectral shape of the single-corner-frequency ω-square source model is then described by the two free parameters M_0 and $\Delta\sigma$. The corner frequency increases with the shear-wave velocity and with increasing stress drop, both of which may be region dependent.

The crustal amplification accounts for the increase in wave amplitude as seismic energy travels through lower- velocity crustal materials from the source to the surface. The amplification depends on average crustal and near surface shear-wave velocity and density (Boore, 1986).

The P(f) filter is used in an attempt to model the observation that acceleration spectral density appears to fall off rapidly beyond some region- or site-dependent maximum frequency (Hanks, 1982; Silva and Darragh, 1995). This observed phenomenon truncates the high frequency portion of the spectrum and is responsible for the band-limited nature of the stochastic model. The band limits are the source corner frequency at low frequency and the high frequency spectral attenuation. This spectral fall-off at high frequency has been attributed to near-site attenuation (Hanks, 1982; Anderson and Hough, 1984) or to source processes (Papageorgiou and Aki, 1983) or perhaps to both effects. In the Anderson and Hough (1984) attenuation model, adopted here, the form of the P(f) filter is taken as

$$P(f, r) = e^{-\pi\kappa(r)f} \qquad \text{(A-4)}.$$

Kappa (r) (κ(r) in Equation A-4) is a site and distance dependent parameter that represents the effect of intrinsic attenuation upon the wavefield as it propagates through the crust from source to receiver. Kappa (r) depends on epicentral distance (r) and on both the shear-wave velocity (β) and quality factor (Q_S) averaged over a depth of H beneath the site (Hough et al., 1988). At zero epicentral distance kappa (κ) is given by

$$\kappa(0) = \frac{H}{\bar{\beta}\,\bar{Q}_S} \qquad \text{(A-5)},$$

and is referred to as κ.

The bar in Equation A-5 represents an average of these quantities over a depth H. The value of kappa at zero epicentral distance is attributed to attenuation in the very shallow crust directly below the site (Hough and Anderson, 1988; Silva and Darragh, 1995). The intrinsic attenuation along this part of the path is not thought to be frequency dependent and is modeled as a frequency independent, but site and crustal region dependent, constant value of kappa (Hough et al., 1988; Rovelli et al., 1988). This zero epicentral distance kappa is the model implemented in this study.

The crustal path attenuation from the source to just below the site is modeled with the frequency- dependent quality factor Q(f). Thus the distance component of the original κ(r) (Equation A-4) is accommodated by Q(f) and R in the last term of Equation A-1:

$$\kappa(r) = \frac{H}{\bar{\beta}\,\bar{Q}_S} + \frac{R}{\beta_0\, Q(f)} \qquad \text{(A-6).}$$

The Fourier amplitude spectrum, a(f), given by Equation A-1 represents the stochastic ground motion model employing a Brune source spectrum that is characterized by a single corner frequency. It is a point source and models direct shear-waves in a homogeneous half-space (with effects of a velocity gradient captured by the A(f) filter, Equation A-1). For horizontal motions, vertically propagating shear-waves are assumed. Validations using incident inclined SH-waves accompanied with raytracing to find appropriate incidence angles leaving the source showed little reduction in uncertainty compared to results using vertically propagating shear-waves. For vertical motions, P/SV propagators are used coupled with raytracing to model incident inclined plane waves (EPRI, 1993). This approach has been validated with recordings from the 1989 **M** 6.9 Loma Prieta earthquake (EPRI, 1993).

Equation A-1 represents an elegant ground motion model that accommodates source and wave propagation physics as well as propagation path and site effects with an attractive simplicity. The model is appropriate for an engineering characterization of ground motion since it captures the general features of strong ground motion in terms of peak acceleration and spectral composition with a minimum of free parameters (Boore, 1983; McGuire et al., 1984; Boore, 1986; Silva and Green, 1988; Silva et al., 1988; Schneider et al., 1993; Silva and Darragh, 1995). An additional important aspect of the stochastic model employing a simple source description is that the region-dependent parameters may be evaluated by observations of small local or regional earthquakes. Region-specific seismic hazard evaluations can then be made for areas with sparse strong motion data with relatively simple spectral analyses of weak motion (Silva, 1992).

In order to compute peak time-domain values, i.e. peak acceleration and oscillator response, RVT is used to relate RMS computations to peak value estimates. Boore (1983) and Boore and Joyner (1984) present an excellent development of the RVT methodology as applied to the stochastic ground motion model. The procedure involves computing the RMS value by integrating the power spectrum from zero frequency to the Nyquist frequency and applying Parsevall's relation. Extreme value theory is then used to estimate the expected ratio of the peak value to the RMS value of a specified duration of the stochastic time history. The duration is taken as the inverse of the source corner frequency (Boore, 1983).

Factors that affect strong ground motions such as surface topography, finite and propagating seismic sources, laterally varying near-surface velocity and Q gradients, and random inhomogeneities along the propagation path are not included in the model. While some or all of these factors are generally present in any observation of ground motion and may exert controlling influences in some cases, the simple stochastic point-source model appears to be robust in predicting median or average properties of ground motion (Boore

1983, 1986; Schneider et al., 1993; Silva and Stark, 1993; Silva et al., 1997). The motivation for comprehensive validation exercises involving many earthquakes with a wide range in magnitudes, rupture distances, and site conditions is to capture unmodeled effects. The unmodeled effects which are random are captured in estimates of model uncertainty and those which are pervasive are captured in the estimates of model bias (see later sections). The combination of realistic, albeit simple, model physics with comprehensive validation exercises makes the stochastic point source ground motion model a powerful predictive and interpretative tool for engineering characterization of strong ground motion.

Finite-source Model Ground Motion Model

In the near-source region of large earthquakes, aspects of a finite-source including rupture propagation, directivity source-receiver geometry, and saturation of high-frequency ($\geq$ 1 Hz) motions with increasing magnitude can be significant and may be incorporated into strong ground motion predictions. To accommodate these effects, a methodology that combines the aspects of finite-earthquake-source modeling techniques (Hartzell, 1978; Irikura 1983) with the stochastic point-source ground motion model has been developed to produce response spectra as well as time histories appropriate for engineering design (Silva et al., 1990; Silva and Stark, 1993; Schneider et al., 1993). The approach is very similar to the empirical Green function methodology introduced by Hartzell (1978) and Irikura (1983). In this case however, the stochastic point-source is substituted for the empirical Green function and peak amplitudes; PGA, PGV, and response spectra (when time histories are not produced) are estimated using random process theory.

Use of the stochastic point-source as a Green function is motivated by its demonstrated success in modeling ground motions in general and strong ground motions in particular (Boore, 1983, 1986; Silva and Stark, 1993; Schneider et al., 1993; Silva and Darragh, 1995) and the desire to have a model that is truly site- and region-specific. The model can accommodate a region specific Q(f), Green function sources of arbitrary moment or stress drop, and site specific kappa values and soil profiles. The necessity for having available regional and site specific recordings distributed over the rupture surface of a future earthquake or modifying possibly inappropriate empirical Green functions is eliminated.

For the finite-source characterization, a rectangular fault is discretized into NS subfaults of moment M_0^S. The empirical relationship

$$\log (A) = \mathbf{M} - 4.0, \quad A \text{ in km}^2 \tag{A-7}$$

is used to assign areas to both the target earthquake (if its rupture surface is not fixed) as well as to the subfaults. This relation results from regressing log area on **M** using the data of Wells and Coppersmith (1994). In the regression, the coefficient on **M** is set to unity which implies a constant static stress drop of about 30 bars (Equation A-9). This is consistent with the general observation of a constant static stress drop for earthquakes based on aftershock locations (Wells and Coppersmith 1994). The static stress drop,

defined by Equation A-10, is related to the average slip over the rupture surface as well as rupture area. It is theoretically identical to the stress drop in Equation A-3 which defines the omega-square source corner frequency assuming the rupture surface is a circular crack model (Brune, 1970; 1971). The stress drop determined by the source corner frequency (or source duration) is usually estimated through the Fourier amplitude spectral density while the static stress drop uses the moment magnitude and an estimate of the rupture area. The two estimates for the same earthquake seldom yield the same values with the static generally being the smaller. In a recent study (Silva et al., 1997), the average stress drop based on Fourier amplitude spectra determined from an empirical attenuation relation (Abrahamson and Silva, 1997) is about 70 bars while the average static stress drop for the crustal earthquakes studied by Wells and Coppersmith (1994) is about 30 bars. These results reflect a general factor of about 2 on average between the two values. These large differences may simply be the result of using an inappropriate estimate of rupture area as the zone of actual slip is difficult to determine unambiguously. In general however, even for individual earthquakes, the two stress drops scale similarly with high static stress drops (> 30 bars) resulting in large high frequency (> 1 Hz for **M** ∃ 5) ground motions which translates to high corner frequencies (Equation A-3).

The subevent magnitude M_S is generally taken in the range of 5.0-6.5 depending upon the size of the target event. M_S 5.0 is used for crustal earthquakes with **M** in the range of 5.5 to 8.0 and M_S 6.4 is used for large subduction earthquakes with **M** > 7.5. The value of NS is determined as the ratio of the target event area to the subfault area. To constrain the proper moment, the total number of events summed (N) is given by the ratio of the target event moment to the subevent moment. The subevent and target event rise times (duration of slip at a point) are determined by the equation

$$\log \tau = 0.33 \log M_0 - 8.54 \qquad \text{(A-8)}$$

which results from a fit to the rise times used in the finite-fault modeling exercises, (Silva et al., 1997). Slip on each subfault is assumed to continue for a time τ. The ratio of target-to-subevent rise times is given by

$$\frac{\tau}{\tau^s} = 10^{0.5\,(\mathrm{M}\,-\,\mathrm{MSUPs})} \qquad \text{(A-9)}$$

and determines the number of subevents to sum in each subfault. This approach is generally referred to as the constant-rise-time model and results in variable slip velocity for nonuniform slip distributions. Alternatively, one can assume a constant slip velocity (as do Beresnev and Atkinson, 2002) resulting in a variable-rise-time model for heterogenous slip distributions. This approach was implemented and validations resulted in an overall "best" average slip velocity of about 70 cm/sec, with no significant improvement over a magnitude dependent rise time (Equation A-8). The feature is retained as an option in the simulation code.

Recent modeling of the Landers (Wald and Heaton, 1994), Kobe (Wald, 1996) and Northridge (Hartzell et al. 1996) earthquakes suggests that a mixture of both constant rise time and constant slip velocity may be present. Longer rise times seem to be associated with areas of larger slip with the ratio of slip-to-rise time (slip velocity) being depth dependent. Lower slip velocities (longer rise times) are associated with shallow slip resulting in relatively less short period seismic radiation. This result may explain the general observation that shallow slip is largely aseismic. The significant contributions to strong ground motions appear to originate at depths exceeding about 4 km (Campbell, 1993; Boore et al., 1994) as the fictitious depth term in empirical attenuation relation (Abrahamson and Silva, 1997; Boore et al., 1997). Finite-fault models generally predict unrealistically large strong ground motions for large shallow (near surface) slip using rise times or slip velocities associated with deeper (> 4 km) zones of slip. This is an important and unresolved issue in finite-fault modeling and the general approach is constrain the slip to relatively small values in the top 2 to 4 km. For the composite source model, the approach is to taper the subevent stress drop to zero at the ground surface (Yehua Zeng, personal communication 1999). A more thorough analysis is necessary, ideally using several well validated models, before this issue can be satisfactorily resolved.

To introduce heterogeneity of the earthquake source process into the stochastic finite-fault model, the location of the sub-events within each subfault (Hartzell, 1978) are randomized as well as the subevent rise time ($\sigma_{ln} = 0.8$). The stress drop of the stochastic point-source Green function is taken as 30 bars, consistent with the static value based on the **M** 5.0 subevent area using the equation

$$\Delta\sigma = \frac{7}{16}\left(\frac{M_e}{R_e^3}\right) \qquad \text{(Brune, 1970, 1971)} \qquad \text{(A-10)}$$

where R_e is the equivalent circular radius of the rectangular sub-event.

Different values of slip are assigned to each subfault as relative weights so that asperities or non-uniform slip can be incorporated into the methodology. For validation exercises, slip models are taken from the literature and are based on inversions of strong motion as well as regional or teleseismic recordings. To produce slip distributions for future earthquakes, random slip models are generated based on a statistical asperity model with parameters calibrated to the published slip distributions. This approach has been validated by comparing the modeling uncertainty and bias estimates for the Loma Prieta and Whittier Narrows earthquakes using motion at each site averaged over several (30) random slip models to the bias and uncertainty estimates using the published slip model. The results show nearly identical bias and uncertainty estimates suggesting that averaging the motions over random slip models produces as accurate a prediction at a site as a single motion computed using the "true" slip model which is determined from inverting actual recordings.

The rupture velocity is taken as depth independent at a value of 0.8 times the shear-wave velocity, generally at the depth of the dominant slip. This value is based on a number of

studies of source rupture processes which also suggest that rupture velocity is non-uniform. To capture the effects of non-uniform rupture velocity, a random component is added through the randomized location of the subevents within each subfault. The radiation pattern is computed for each subfault, a random component added, and the RMS applied to the motions computed at the site when modeling an average horizontal component. To model individual horizontal components, the radiation pattern for each subfault is used to scale each subfaults contribution to the final summed motion.

The ground-motion time history at the receiver is computed by summing the contributions from each subfault associated with the closest Green function, transforming to the frequency domain, and convolving with the appropriate Green function spectrum (Equation A-1). The locations of the Green functions are generally taken at center of each subfault for small subfaults or at a maximum separation of about 5 to 10 km for large subfaults. As a final step, the individual contributions associated with each Green function are summed in the frequency domain, multiplied by the RMS radiation pattern, and the resultant power spectrum at the site is computed. The appropriate duration used in the RVT computations for PGA, PGV, and oscillator response is computed by transforming the summed Fourier spectrum into the time domain and computing the 5 to 75% Arias intensity (Ou and Herrmann, 1990).

As with the point-source model, crustal response effects are accommodated through the amplification factor (A(f)) or by using vertically propagating shear waves through a vertically heterogenous crustal structure. Propagation path damping, through the Q(f) model, is incorporated from each fault element to the site. Near-surface crustal damping is incorporated through the kappa operator (Equation A-1). To model crustal propagation path effects, the raytracing method of Ou and Herrmann (1990) is applied from each subfault to the site.

Time histories may be computed in the process as well by simply adding a phase spectrum appropriate to the subevent earthquake. The phase spectrum can be extracted from a recording made at close distance to an earthquake of a size comparable to that of the subevent (generally **M** 5.0 to 6.5). Interestingly, the phase spectrum need not be from a recording in the region of interest (Silva et al., 1989). A recording in WNA (Western North America) can effectively be used to simulate motions appropriate to ENA (Eastern North America). Transforming the Fourier spectrum computed at the site into the time domain results in a computed time history which then includes all of the aspects of rupture propagation and source finiteness, as well as region specific propagation path and site effects.

For fixed fault size, mechanism, and moment, the specific source parameters for the finite-fault are slip distribution, location of nucleation point, and site azimuth. The propagation path and site parameters remain identical for both the point- and finite-source models.

Partition and assessment of ground motion variability

APPENDIX A

An essential requirement of any numerical modeling approach, particularly one which is implemented in the process of defining design ground motions, is a quantative assessment of prediction accuracy. A desirable approach to achieving this goal is in a manner which lends itself to characterizing the variability associated with model predictions. For a ground motion model, prediction variability is comprised of two components: modeling variability and parametric variability. Modeling variability is a measure of how well the model works (how accurately it predicts ground motions) when specific parameter values are known. Modeling variability is measured by misfits of model predictions to recorded motions through validation exercises and is due to unaccounted for components in the source, path, and site models (i.e. a point-source cannot model the effects of directivity and linear site response cannot accommodate nonlinear effects). Results from a viable range of values for model parameters (i.e., slip distribution, soil profile, G/G_{max} and hysteretic damping curves, etc). Parametric variability is the sensitivity of a model to a viable range of values for model parameters. The total variability, modeling plus parametric, represents the variance associated with the ground motion prediction and, because it is a necessary component in estimating fractile levels, may be regarded as important as median predictions.

Both the modeling and parametric variabilities may have components of randomness and uncertainty. Table A.1 summarizes the four components of total variability in the context of ground motion predictions. Uncertainty is that portion of both modeling and parametric variability which, in principle, can be reduced as additional information becomes available, whereas randomness represents the intrinsic or irreducible component of variability for a given model or parameter. Randomness is that component of variability which is intrinsic or irreducible <u>for a given model.</u> The uncertainty component reflects a lack of knowledge and may be reduced as more data are analyzed. For example, in the point-source model, stress drop is generally taken to be independent of source mechanism as well as tectonic region and is found to have a standard error of about 0.7 (natural log) for the CEUS (EPRI, 1993). This variation or uncertainty plus randomness in $\Delta\sigma$ results in a variability in ground motion predictions for future earthquakes. If, for example, it is found that normal faulting earthquakes have generally lower stress drops than strike-slip which are, in turn, lower than reverse mechanism earthquakes, perhaps much of the variability in $\Delta\sigma$ may be reduced. In extensional regimes, where normal faulting earthquakes are most likely to occur, this new information may provide a reduction in variability (uncertainty component) for stress drop, say to 0.3 or 0.4 resulting in less ground motion variation due to a lack of knowledge of the mean or median stress drop. There is, however, a component of this stress drop variability which can <u>never</u> be reduced in the context of the Brune model. This is simply due to the heterogeneity of the earthquake dynamics which is not accounted for in the model and results in the randomness component of parametric variability in stress drop. A more sophisticated model may be able to accommodate or model more accurately source dynamics but, perhaps, at the expense of a larger number of parameters and increased parametric uncertainty (i.e. the finite-fault with slip model and nucleation point as unknown parameters for future earthquakes). That is, more complex models typically seek to reduce modeling randomness by more closely modeling physical phenomena. However, such models often require more comprehensive sets of observed data to constrain additional model parameters, which

generally leads to increased parametric variability. If the increased parametric variability is primarily in the form of uncertainty, it is possible to reduce total variability, but only at the additional expense of constraining the additional parameters. Therefore, existing knowledge and/or available resources may limit the ability of more complex models to reduce total variability.

The distinction of randomness and uncertainty is model driven and somewhat arbitrary. The allocation is only important in the context of probabilistic seismic hazard analyses as uncertainty is treated as alternative hypotheses in logic trees while randomness is integrated over in the hazard calculation (Cornell, 1968). For example, the uncertainty component in stress drop may be treated by using an N-point approximation to the stress drop distribution and assigning a branch in a logic tree for each stress drop and associated weight. A reasonable three point approximation to a normal distribution is given by weights of 0.2, 0.6, 0.2 for expected 5%, mean, and 95% values of stress drop respectively. If the distribution of uncertainty in stress drop was such that the 5%, mean, and 95% values were 50, 100, and 200 bars respectively, the stress drop branch on a logic tree would have 50, and 200 bars with weights of 0.2 and 100 bars with a weight of 0.6. The randomness component in stress drop variability would then be formally integrated over in the hazard calculation.

Assessment of Modeling Variability

Modeling variability (uncertainty plus randomness) is usually evaluated by comparing response spectra computed from recordings to predicted spectra and is a direct assessment of model accuracy. The modeling variability is defined as the standard error of the residuals of the log of the average horizontal component (or vertical component) response spectra. The residual is defined as the difference of the logarithms of the observed average 5% damped acceleration response spectra and the predicted response spectra. At each period, the residuals are squared, and summed over the total number of sites for one or all earthquakes modeled. Dividing the resultant sum by the number of sites results in an estimate of the model variance. Any model bias (average offset) that exists may be estimated in the process (Abrahamson et al., 1990; EPRI, 1993) and used to correct (lower) the variance (and to adjust the median as well). In this approach, the modeling variability can be separated into randomness and uncertainty where the bias corrected variability represents randomness and the total variability represents randomness plus uncertainty. The uncertainty is captured in the model bias as this may be reduced in the future by refining the model. The remaining variability (randomness) remains irreducible for this model. In computing the variance and bias estimates only the frequency range between processing filters at each site (minimum of the 2 components) should be used.

Assessment of Parametric Variability

Parametric variability, or the variation in ground motion predictions due to uncertainty and randomness in model parameters is difficult to assess. Formally, it is straight-forward in that a Monte Carlo approach may be used with each parameter randomly sampled about its mean (median) value either individually for sensitivity analyses (Silva,

1992; Roblee et al., 1996) or in combination to estimate the total parametric variability (Silva, 1992; EPRI, 1993). In reality, however, there are two complicating factors.

The first factor involves the specific parameters kept fixed with all earthquakes, paths, and sites when computing the modeling variability. These parameters are then implicitly included in modeling variability provided the data sample a sufficiently wide range in source, path, and site conditions. The parameters which are varied during the assessment of modeling variation should have a degree of uncertainty and randomness associated with them for the next earthquake. Any ground motion prediction should then have a variation reflecting this lack of knowledge and randomness in the free parameters.

An important adjunct to fixed and free parameters is the issue of parameters which may vary but by fixed rules. For example, source rise time (Equation A-8) is magnitude dependent and in the stochastic finite-source model is specified by an empirical relation. In evaluating the modeling variability with different magnitude earthquakes, rise time is varied, but because it follows a strict rule, any variability associated with rise time variation is counted in modeling variability. This is strictly true only if the sample of earthquakes has adequately spanned the space of magnitude, source mechanism, and other factors which may affect rise time. Also, the earthquake to be modeled must be within that validation space. As a result, the validation or assessment of model variation should be done on as large a number of earthquakes of varying sizes and mechanisms as possible.

The second, more obvious factor in assessing parametric variability is a knowledge of the appropriate distributions for the parameters (assuming correct values for median or mean estimates are known). In general, for the stochastic models, median parameter values and uncertainties are based, to the extent possible, on evaluating the parameters derived from previous earthquakes (Silva, 1992; EPRI, 1993).

The parametric variability is site, path, and source dependent and must be evaluated for each modeling application (Roblee et al., 1996). For example, at large source-to-site distances, crustal path damping may control short-period motions. At close distances to a large fault, both the site and finite-source (asperity location and nucleation point) may dominate, and, depending upon site characteristics, the source or site may control different frequency ranges (Silva, 1992; Roblee et al., 1996). Additionally, level of control motion may affect the relative importance of G/G_{max} and hysteretic damping curves.

In combining modeling and parametric variations, independence is assumed (covariance is zero) and the variances are simply added to give the total variability.

$$_{ln}\sigma^2_T = {}_{ln}\sigma^2_M + {}_{ln}\sigma^2_P{}^2 \qquad \text{(A-11)},$$

[2]Strong ground motions are generally considered to be log normally distributed.

where

$_{ln}\sigma^2_M$ = modeling variation,

$_{ln}\sigma^2_P$ = parametric variation.

Validation Of The Point- and Finite-Source Models

In a recent Department of Energy sponsored project (Silva et al., 1997), both the point- and finite-source stochastic models were validated in a systematic and comprehensive manner. In this project, 16 well recorded earthquakes were modeled at about 500 sites. Magnitudes ranged from **M** 5.3 to **M** 7.4 with fault distances from about 1 km out to 218 km for WUS earthquakes and 460 km for CEUS earthquakes. This range in magnitude and distance as well as number of earthquakes and sites results in the most comprehensively validated model currently available to simulate strong ground motions.

For these exercises, regional Q(f) models and point source stress drops were determined through inversions using the strong motion recordings (Silva et al., 1997). Small strain WUS rock and soil kappa values were set to 0.04 sec, the average from the inversions of small strain data. CEUS rock site kappa values were fixed at inversion values, which averaged about 0.02 sec and ranged from 0.004 to 0.06 sec. For the finite source parameters, slip models and nucleation points were taken from the literature (Silva et al., 1997). Point-source depths were taken as the depth of the center of the largest asperity in the slip models while point-source distance used the closest distance to the surface projection of the rupture surface.

A unique aspect of this validation is that rock and soil sites were modeled using generic rock and soil profiles and equivalent-linear site response. Validations done with other simulation procedures typically neglect site conditions as well as nonlinearity resulting in ambiguity in interpretation of the simulated motions.

Point-Source Model

Final model bias and variability estimates for the point-source model are shown in Figure A1. Over all the sites (Figure A1) the bias is slightly positive for frequencies greater than about 10 Hz and is near zero from about 10 Hz to 1 Hz. Below 1 Hz, a stable point-source overprediction is reflected in the negative bias. The analyses are considered reliable down to about 0.3 Hz (3.3 sec) where the point-source shows about a 40% overprediction.

The model variability is low, about 0.5 above about 3 to 4 Hz and increases with decreasing frequency to near 1 at 0.3 Hz. Above 1 Hz, there is little difference between the total variability (uncertainty plus randomness) and randomness (bias corrected

variability) reflecting the near zero bias estimates. Below 1 Hz there is considerable uncertainty contributing to the total variability suggesting that the model can be measurably improved as its predictions tend to be consistently high at very low frequencies (# 1 Hz). This stable misfit may be interpreted as the presence of a second corner frequency for WNA sources (Atkinson and Silva, 1997).

Finite-Source Model

For the finite-fault, Figure A2 shows the corresponding bias and variability estimates. For all the sites, the finite-source model provides slightly smaller bias estimates and, surprisingly, slightly higher variability for frequencies exceeding about 5 Hz. The low frequency (# 1 Hz) point-source overprediction is not present in the finite-source results, indicating that it is giving more accurate predictions than the point-source model over a broad frequency range, from about 0.3 Hz (the lowest frequency of reliable analyses) to the highest frequency of the analyses.

In general, for frequencies of about 1 Hz and above the point-source and finite-source give comparable results: the bias estimates are small (near zero) and the variabilities range from about 0.5 to 0.6. These estimates are low considering the analyses are based on a data set comprised of earthquakes with **M** less than **M** 6.5 (288 of 513 sites) and high frequency ground motion variance decreases with increasing magnitude, particularly above **M** 6.5 (Youngs et al., 1995) Additionally, for the vast majority of sites, generic site conditions were used (inversion kappa values were used for only the Saguenay and Nahanni earthquake analyses, 25 rock sites). As a result, the model variability (mean = 0) contains the total uncertainty and randomness contribution for the site. The parametric variability due to uncertainty and randomness in site parameters: shear-wave velocity, profile depth, G/G_{max} and hysteretic damping curves need not be added to the model variability estimates. It is useful to perform parametric variations to assess site parameter sensitivities on the ground motions, but only source and path damping Q(f) parametric variabilities require assessment on a site specific basis and added to the model variability. The source uncertainty and randomness components include point-source stress drop as well as source depth and finite-source slip model and nucleation point (Silva, 1992).

The general approach taken in these validations is to have few free parameters and accept a relatively large model misfit. This approach relaxes the need to develop appropriate distributions for poorly resolved parameters such as spatially varying rise times and rupture velocity as well as non-planar rupture surfaces (e.g. Landers, Kobe, and Kocaeli earthquakes). An alternative approach is to adjust these suites of parameters, which naturally improves the fits to recorded motions and results in smaller modeling uncertainties. However, unless independent information is available to constrain these parameters for future earthquakes, they must be appropriately counted as parametric variability. This may result in the total variability remaining comparable between the two approaches. This concept parallels the utility of increased model complexity, i.e., simple verses complex models. More complex models may increase an understanding of physical processes but, in the context of predicting motions due to the next earthquake, increased model complexity may not provide more accurate estimates of strong ground

motions, again unless independent information is available to constrain potential ranges in some or all of the free parameters.

A summary of fixed and free parameters for the implementation of the stochastic point and finite source models presented here is listed in Table 2.

Empirical Attenuation Model

As an additional assessment of the stochastic models, bias and variability estimates were made over the same earthquakes (except Saguenay since it was not used in the regressions) and sites using a recently develop empirical attenuation relation (Abrahamson and Silva, 1997). For all the sites, the estimates are shown in Figure A3. Interestingly, the point-source overprediction below about 1 Hz is present in the empirical relation perhaps suggesting that this suite of earthquakes possess lower than expected motions in this frequency range as the empirical model does not show this bias over all earthquakes (. 50) used in its development. Comparing these results to the point- and finite-source results (Figures A1 and A2) show comparable bias and variability estimates. For future predictions, source and path damping parametric variability must be added to the numerical simulations which will contribute a σ_{ln} of about 0.2 to 0.4, depending upon frequency, source and path conditions, and site location. This will raise the modeling variability from about 0.50 to the range of 0.54 to 0.64, about 10 to 30%. These values are still comparable to the variability of the empirical relation indicating that the point- and finite-source numerical models perform about as well as a recently developed empirical attenuation relation for the validation earthquakes and sites.

These results are very encouraging and provide an additional qualitative validation of the point- and finite-source models. Paranthetically this approach provides a rational basis for evaluating empirical attenuation models.

APPENDIX A

REFERENCES

Abrahamson, N.A. and W.J. Silva (1997). "Empirical response spectral attenuation relations for shallow crustal earthquakes." *Seismological Research Let.,* 68(1), 94-127.

Abrahamson, N.A., P.G. Somerville, and C.A. Cornell (1990). "Uncertainty in numerical strong motion predictions" *Proc. Fourth U.S. Nat. Conf. Earth. Engin.*, Palm Springs, CA., 1, 407-416.

Aki, K. and P.G. Richards. (1980). *"Quantitative siesmology."* W. H. Freeman and Co., San Francisco, California.

Atkinson, G.M and W.J. Silva (1997). "An empirical study of earthquake source spectra for California earthquakes." *Bull. Seism. Soc. Am.* 87(1), 97-113.

Anderson, J.G. and S.E. Hough (1984). "A Model for the Shape of the Fourier Amplitude Spectrum of Acceleration at High Frequencies." *Bulletin of the Seismological Society of America,* 74(5), 1969-1993.

Atkinson, G.M. (1984). "Attenuation of strong ground motion in Canada from a random vibrations approach." *Bull. Seism. Soc. Am.*, 74(5), 2629-2653.

Beresnev, I.A. and G. M. Atkinson (2002). "Source parameters of earthquakes in Eastern and Western North America." *Bull. Seism. Soc. Am.,* 92(2), 695-710.

Boore, D.M., W.B. Joyner, and T.E. Fumal (1997). "Equations for estimating horizontal response spectra and peak acceleration from Western North American earthquakes: A summary of recent work." *Seism. Res. Lett.* 68(1), 128-153.

Boore, D.M., W.B. Joyner, and T.E. Fumal (1994). "Estimation of response spectra and peak accelerations from western North American earthquakes: and interim report. Part 2. *U.S. Geological Survey Open-File Rept.* 94-127.

Boore, D.M., and G.M. Atkinson (1987). "Stochastic prediction of ground motion and spectral response parameters at hard-rock sites in eastern North America." *Bull. Seism. Soc. Am.*, 77(2), 440-467.

Boore, D.M. (1986). "Short-period P- and S-wave radiation from large earthquakes: implications for spectral scaling relations." *Bull. Seism. Soc. Am.*, 76(1) 43-64.

Boore, D.M. and W.B. Joyner (1984). "A note on the use of random vibration theory to predict peak amplitudes of transient signals." *Bull. Seism. Soc. Am.*, 74, 2035-2039.

Boore, D.M. (1983). "Stochastic simulation of high-frequency ground motions based on seismological models of the radiated spectra." *Bull. Seism. Soc. Am.*, 73(6), 1865-1894.

Brune, J.N. (1971). "Correction." *J. Geophys. Res.* 76, 5002.

Brune, J.N. (1970). "Tectonic stress and the spectra of seismic shear waves from earthquakes." *J. Geophys. Res.* 75, 4997-5009.

Campbell, K.W. (1993) "Empirical prediction of near-source ground motion from large earthquakes." in V.K. Gaur, ed., *Proceedings, Intern'l Workshop on Earthquake Hazard and Large Dams in the Himalya.* INTACH, New Delhi, p. 93-103.

Cornell, C.A. (1968). "Engineering seismic risk analysis." *Bull. Seism. Soc. Am.*, 58, 1583-1606.

Electric Power Research Institute (1993). "Guidelines for determining design basis ground motions." Palo Alto, Calif: Electric Power Research Institute, vol. 1-5, EPRI TR-102293.

vol. 1: Methodology and guidelines for estimating earthquake ground motion in eastern North America.
vol. 2: Appendices for ground motion estimation.
vol. 3: Appendices for field investigations.
vol. 4: Appendices for laboratory investigations.
vol. 5: Quantification of seismic source effects.

Hanks, T.C. (1982). "f_{max}." *Bull. Seism. Soc. Am.,* 72, 1867-1879.

Hanks, T.C. and R.K. McGuire (1981). "The character of high-frequency strong ground motion." *Bull. Seism. Soc. Am.*, 71(6), 2071-2095.

Hanks, T.C. and H. Kanamori (1979). "A moment magnitude scale." *J. Geophys. Res.*, 84, 2348-2350.

Hartzell, S., A. Leeds, A. Frankel, and J. Michael (1996). "Site response for urban Los Angeles using aftershocks of the Northridge earthquake." *Bull. Seism. Soc. Am.*, 86(1B), S168-S192.

Hartzell, S.H. (1978). "Earthquake aftershocks as Green's functions." *Geophys. Res. Letters*, 5, 1-4.

Hough, S.E., J.G. Anderson, J. Brune, F. Vernon III, J. Berger, J. Fletcher, L. Haar, T. Hanks, and L. Baker (1988). "Attenuation near Anza, California." *Bull. Seism. Soc. Am.*, 78(2), 672-691.

Hough, S.E. and J.G. Anderson (1988). "High-Frequency Spectra Observed at Anza, California: Implications for Q Structure." *Bull. Seism. Soc. Am.*, 78(2), 692-707.

Irikura, K. (1983). "Semi-empirical estimation of strong ground motions during large earthquakes." *Bull. Disaster Prevention Res. Inst.*, Kyoto Univ., 33, 63-104.

McGuire, R. K., A.M. Becker, and N.C. Donovan (1984). "Spectral Estimates of Seismic Shear Waves." *Bull. Seism. Soc. Am.*, 74(4), 1427-1440.

Ou, G.B. and R.B. Herrmann (1990). "Estimation theory for strong ground motion." *Seism. Res. Letters.* 61.

Papageorgiou, A.S. and K. Aki (1983). "A specific barrier model for the quantitative description of inhomogeneous faulting and the prediction of strong ground motion, part I, Description of the model." *Bull. Seism. Soc. Am.*, 73(4), 693-722.

Roblee, C.J., W.J. Silva, G.R. Toro and N. Abrahamson (1996). "Variability in site-specific seismic ground-motion design predictions." in press.

Rovelli, A., O. Bonamassa, M. Cocco, M. Di Bona, and S. Mazza (1988). "Scaling laws and spectral parameters of the ground motion in active extensional areas in Italy." *Bull. Seism. Soc. Am.*, 78(2), 530-560.

Schneider, J.F., W.J. Silva, and C.L. Stark (1993). "Ground motion model for the 1989 **M** 6.9 Loma Prieta earthquake including effects of source, path and site." *Earthquake Spectra*, 9(2), 251-287.

Silva, W.J., N. Abrahamson, G. Toro, and C. Costantino (1997). "Description and validation of the stochastic ground motion model." Submitted to Brookhaven National Laboratory, Associated Universities, Inc. Upton, New York.

Silva, W.J. and R. Darragh (1995). "Engineering characterization of earthquake strong ground motion recorded at rock sites." Palo Alto, Calif:Electric Power Research Institute, TR-102261.

Silva, W.J. and C.L. Stark (1993) "Source, path, and site ground motion model for the 1989 **M** 6.9 Loma Prieta earthquake." CDMG draft final report.

Silva, W.J. (1992). "Factors controlling strong ground motions and their associated uncertainties." *Dynamic Analysis and Design Considerations for High Level Nuclear Waste Repositories, ASCE* 132-161.

Silva, W.J. (1991). "Global characteristics and site geometry." Chapter 6 in *Proceedings: NSF/EPRI Workshop on Dynamic Soil Properties and Site Characterization.* Palo Alto, Calif.: Electric Power Research Institute, NP-7337.

Silva, W. J., R. Darragh, C. Stark, I. Wong, J. C. Stepp, J. Schneider, and S-J. Chiou (1990). "A Methodology to Estimate Design Response Spectra in the Near-Source Region of Large Earthquakes Using the Band-Limited-White-Noise Ground Motion Model". *Procee. of the Fourth U.S. Conf. on Earthquake Engineering,* Palm Springs, California. 1, 487-494.

Silva, W.J., R.B. Darragh, R.K. Green and F.T. Turcotte (1989). *Estimated Ground Motions for a new madrid Event.* U.S. Army Engineer Waterways Experiment Station, Wash., DC, Misc. Paper GL-89-17.

Silva, W. J. and R. K. Green (1988). "Magnitude and Distance Scaling of Response Spectral Shapes for Rock Sites with Applications to North American Environments." In *Proceedings: Workshop on Estimation of Ground Motion in the Eastern United States*, EPRI NP-5875, Electric Power Research Institute.

Silva, W. J., T. Turcotte, and Y. Moriwaki (1988). "Soil Response to Earthquake Ground Motion," Electric Power Research Institute, Walnut Creek, California, Report No. NP-5747.

Silva, W.J. and K. Lee (1987). "*WES RASCAL code for synthesizing earthquake ground motions.*" State-of-the-Art for Assessing Earthquake Hazards in the United States, Report 24, U.S. Army Engineers Waterways Experiment Station, Miscellaneous Paper S-73-1.

Somerville, P.G., R. Graves and C. Saikia (1995). "TECHNICAL REPORT: Characterization of ground motions during the Northridge earthquake of January 17, 1994." *Structural Engineers Association of California (SEAOC).* Report No. SAC-95-03.

Toro, G. R. and R. K. McGuire (1987). "An Investigation into Earthquake Ground Motion Characteristics in Eastern North America." *Bull. Seism. Soc. Am.*, 77(2), 468-489.

Toro, G. R. (1985). "Stochastic Model Estimates of Strong Ground Motion." In *Seismic Hazard Methodology for Nuclear Facilities in the Eastern United States*, Appendix B, R. K. McGuire, ed., Electric Power Research Institute, Project P101-29.

Wald, D.J. (1996). "Slip history of the 1995 Kobe, Japan, earthquake determined from strong motion, teleseismic, and geodetic data." *J. of Physics of the Earth,* in press.

Wald, D.J. and T.H. Heaton (1994). "Spatial and temporal distribution of slip for the 1992 Landers, California, earthquake." *Bull. Seism. Soc. Amer.*, 84(3), 668-691.

Wells, D.L. and K.J. Coppersmith (1994). "New empirical relationships among magnitude, rupture length, rupture width, rupture area, and surface displacement." *Bull. Seism. Soc. Am.* 84(4), 974-1002.

Youngs, R.R., N.A. Abrahamson, F. Makdisi, and K. Sadigh (1995). "Magnitude dependent dispersion in peak ground acceleration." *Bull. Seism. Soc. Amer.*, 85(1), 161-1, 176.

Table A.1

CONTRIBUTIONS TO TOTAL VARIABILITY
IN GROUND MOTION MODELS

	Modeling Variability	Parametric Variability
Uncertainty *(also Epistemic Uncertainty)*	Modeling Uncertainty: Variability in predicted motions resulting from particular model assumptions, simplifications and/or fixed parameter values. *Can be reduced by adjusting or "calibrating" model to better fit observed earthquake response.*	Parametric Uncertainty: Variability in predicted motions resulting from incomplete data needed to characterize parameters. *Can be reduced by collection of additional information which better constrains parameters*
Randomness *(also Aleatory Uncertainty)*	Modeling Randomness: Variability in predicted motions resulting from discrepancies between model and actual complex physical processes. *Cannot be reduced for a given model form.*	Parametric Randomness: Variability in predicted motions resulting from inherent randomness of parameter values. *Cannot be reduced a priori*[***] *by collection of additional information.*

[***]Some parameters (e.g. source characteristics) may be well defined after an earthquakes.

Table A.2

FIXED AND FREE PARAMETERS

Fixed Parameters

Regional Curstal Model
Rock and Soil Generic Profiles
Kappa
G/Gmax and Hysteric Damping Curves
Finite Source Rise Time
Finite Source Rupture Velocity

Free Parameters

Regional Q(f) Model
Point Source Stress Drop and Depth
Finite Source Slip Model and Nucleation Point

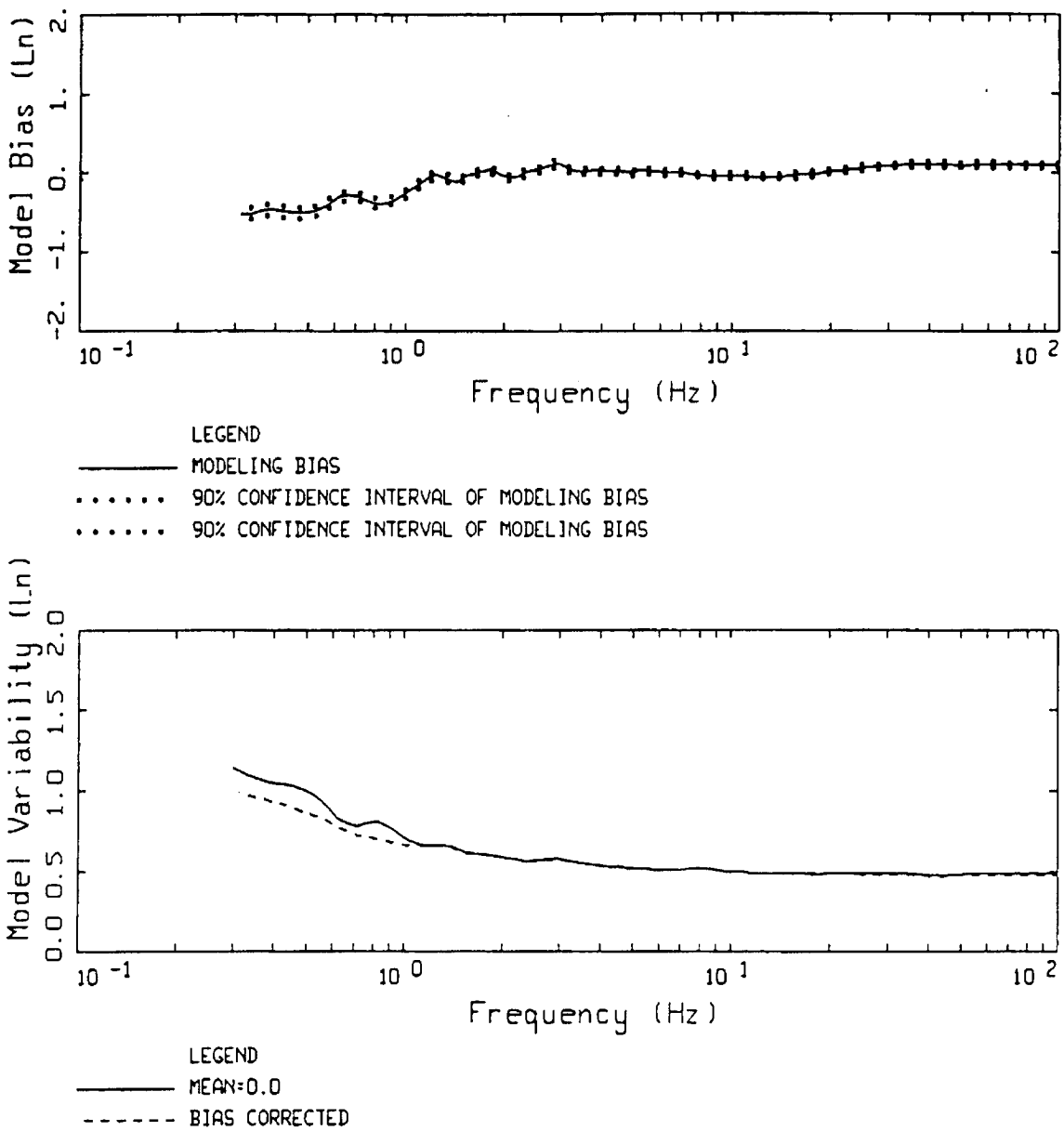

Figure A1. Model bias and variability estimates for all earthquakes computed over all 503 sites for the point-source model.

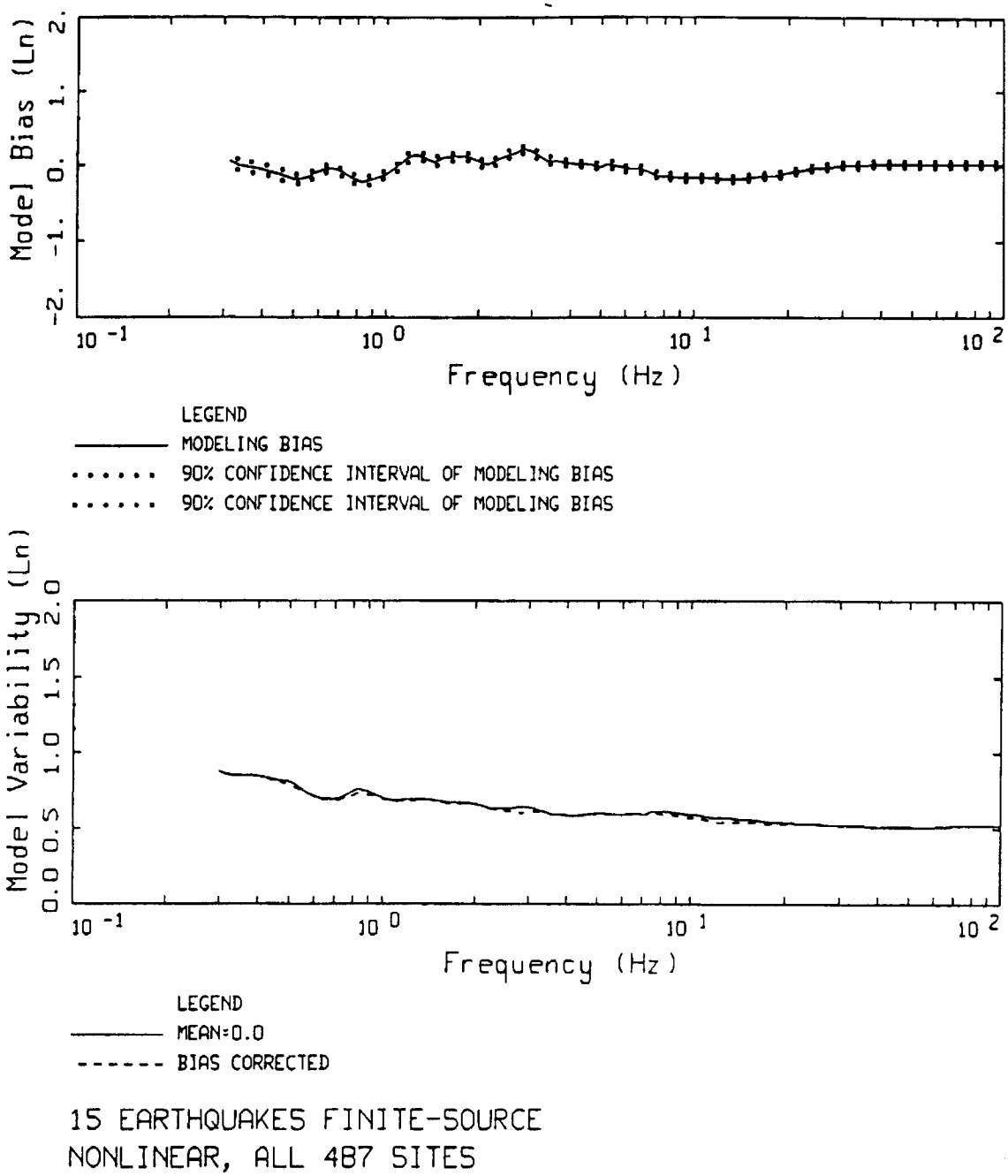

Figure A2. Model bias and variability estimates for all earthquakes computed over all 487 sites for the finite-source model.

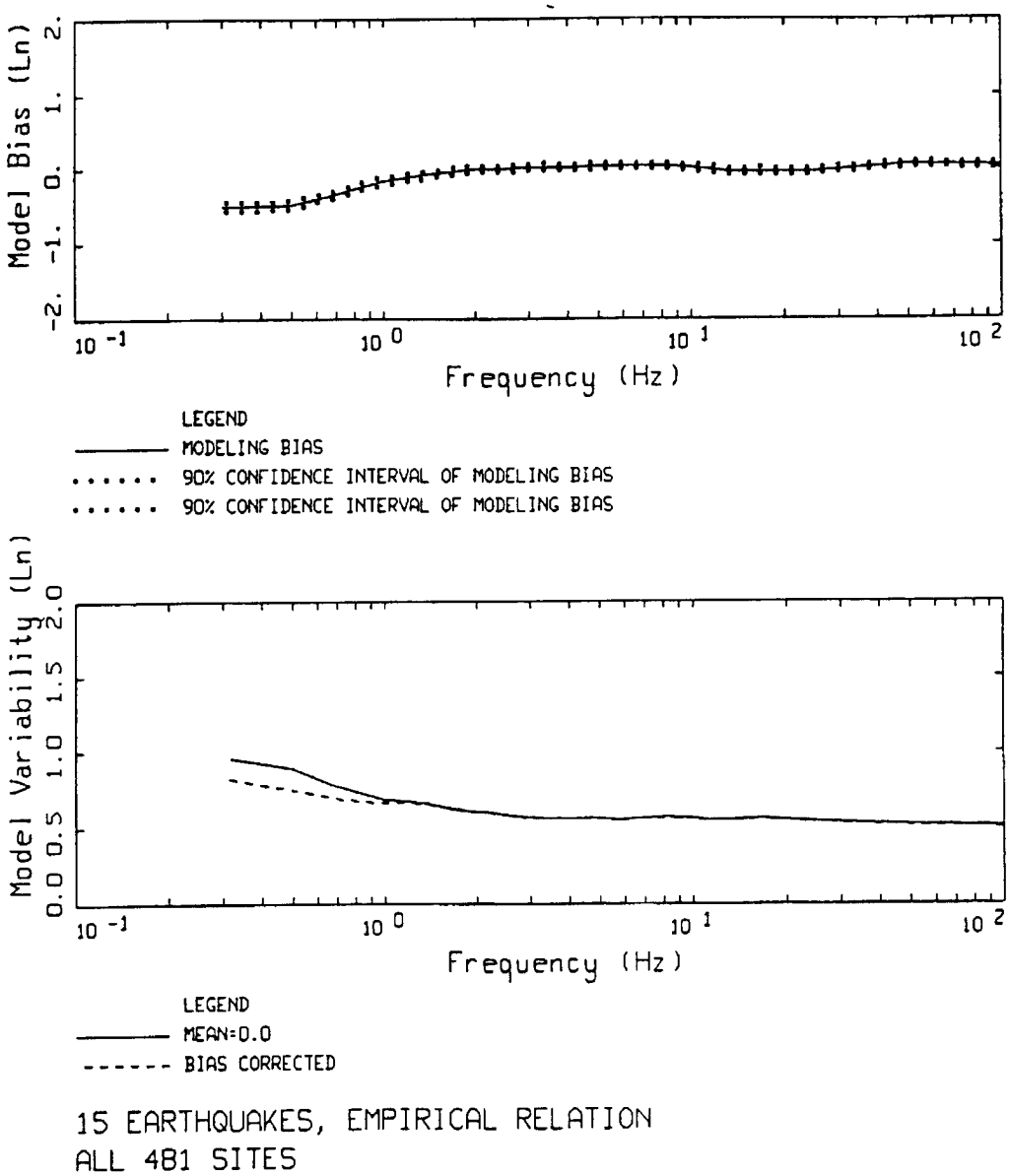

Figure A3. Model bias and variability estimates for all earthquakes computed over all 481 sites for the empirical model.

APPENDIX B

SITE RESPONSE ANALYSIS METHOD

Development of Site Specific Soil Motions

The conventional approach to estimating the effects of site-specific site conditions on strong ground motions involves development of a set (1, 2, or 3 component) of time histories compatible with the specified outcrop response spectra to serve as control (or input) motions. The control motions are then used to drive a nonlinear computational formulation to transmit the motions through the profile. Simplified analyses generally assume vertically propagating shear-waves for horizontal components and vertically propagating compression-waves for vertical motions. These are termed one-dimensional site response analyses.

Equivalent-Linear Computational Scheme

The computational scheme which has been most widely employed to evaluate one-dimensional site response assumes vertically-propagating plane shear-waves. Departures of soil response from a linear constitutive relation are treated in an approximate manner through the use of the equivalent-linear approach.

The equivalent-linear approach, in its present form, was introduced by Seed and Idriss (1970). This scheme is a particular application of the general equivalent-linear theory developed by Iwan (1967). Basically, the approach is to approximate a second order nonlinear equation, over a limited range of its variables, by a linear equation. Formally this is done in such a way that the average of the difference between the two systems is minimized. This was done in an ad-hoc manner for ground response modeling by defining an effective strain which is assumed to exist for the duration of the excitation. This value is usually taken as 65% of the peak time-domain strain calculated at the midpoint of each layer, using a linear analysis. Modulus reduction and hysteretic damping curves are then used to define new parameters for each layer based on the effective strain computations. The linear response calculation is repeated, new effective strains evaluated, and iterations performed until the changes in parameters are below some tolerance level. Generally a few iterations are sufficient to achieve a strain-compatible linear solution.

This stepwise analysis procedure was formalized into a one-dimensional, vertically propagating shear-wave code called SHAKE (Schnabel et al., 1972). Subsequently, this code has easily become the most widely used analysis package for one-dimensional site response calculations.

The advantages of the equivalent-linear approach are that parameterization of complex nonlinear soil models is avoided and the mathematical simplicity of a linear analysis is preserved. A truly nonlinear approach requires the specification of the shapes of hysteresis curves and their cyclic dependencies through an increased number of material parameters. In the equivalent-linear methodology the soil data are utilized directly and, because at each iteration the problem is linear and the material properties are frequency independent, the damping is rate independent and hysteresis loops close.

Careful validation exercises between equivalent-linear and fully nonlinear formulations using recorded motions from 0.05 to 0.50g showed little difference in results (EPRI, 1993). Both formulations compared very favorably to recorded motions suggesting both the adequacy of the vertically propagating shear-wave model and the approximate equivalent-linear formulation. While the assumptions of vertically propagating shear-waves and equivalent-linear soil response certainly represent approximations to actual conditions, their combination has achieved demonstrated success in modeling observations of site effects and represent a stable, mature, and reliable means of estimating the effects of site conditions on strong ground motions (Schnabel et al., 1972; Silva et al., 1988; Schneider et al., 1993; EPRI, 1993).

To accommodate both uncertainty and randomness in dynamic material properties, analyses are typically done for the best estimate shear-wave velocity profile as well as upper- and lower-range profiles. The upper- and lower-ranges are usually specified as twice and one-half the best estimate shear-wave moduli. Depending upon the nature of the structure, the final design spectrum is then based upon an envelope or average of the three spectra.

For vertical motions, the SHAKE code is also used with compression-wave velocities and damping substituted for the shear-wave values. To accommodate possible nonlinear response on the vertical component, since modulus reduction and hysteretic damping curves are not generally available for the constrained modulus, the low-strain Poisson's ratio is usually fixed and strain compatible compression-wave velocities calculated using the strain compatible shear moduli from the horizontal component analyses combined with the low-strain Poisson's ratios. In a similar manner, strain compatible compression-wave damping values are estimated by combining the strain compatible shear-wave damping values with the low-strain damping in bulk or pure volume change. This process assumes the loss in bulk (volume change) is constant or strain independent. Alternatively, zero loss in bulk is assumed and the equation relating shear- and compression-wave damping (η_S and η_P) and velocities (V_S and V_P)

$$\eta_P \approx \frac{4}{3}\frac{V_S}{V_P}\eta_S, \qquad \text{(B-1)}$$

is used.

RVT Based Computational Scheme

The computational scheme employed to compute the site response for this project uses an alternative approach employing random vibration theory (RVT). In this approach the control motion power spectrum is propagated through the one-dimensional soil profile using the plane-wave propagators of Silva (1976). In this formulation only SH waves are

considered. Arbitrary angles of incidence may be specified but normal incidence is used throughout the present analyses.

In order to treat possible material nonlinearities, an RVT based equivalent-linear formulation is employed. Random process theory is used to predict peak time domain values of shear-strain based upon the shear-strain power spectrum. In this sense the procedure is analogous to the program SHAKE except that peak shear-strains in SHAKE are measured in the time domain. The purely frequency domain approach obviates a time domain control motion and, perhaps just as significant, eliminates the need for a suite of analyses based on different input motions. This arises because each time domain analysis may be viewed as one realization of a random process. Different control motion time histories reflecting different time domain characteristics but with nearly identical response spectra can result in different nonlinear and equivalent-linear response.

In this case, several realizations of the random process must be sampled to have a statistically stable estimate of site response. The realizations are usually performed by employing different control motions with approximately the same level of peak accelerations and response spectra.

In the case of the frequency domain approach, the estimates of peak shear-strain as well as oscillator response are, as a result of the random process theory, fundamentally probabilistic in nature. For fixed material properties, stable estimates of site response can then be obtained with a single run.

In the context of the RVT equivalent-linear approach, a more robust method of incorporating uncertainty and randomness of dynamic material properties into the computed response has been developed. Because analyses with multiple time histories are not required, parametric variability can be accurately assessed through a Monte Carlo approach by randomly varying dynamic material properties. This results in median as well as other fractile levels (e.g. 16^{th}, mean, 84^{th}) of smooth response spectra at the surface of the site. The availability of fractile levels reflecting randomness and uncertainty in dynamic material properties then permits a more rational basis for selecting levels of risk.

In order to randomly vary the shear-wave velocity profile, a profile randomization scheme has been developed which varies both layer velocity and thickness. The randomization is based on a correlation model developed from an analysis of variance on about 500 measured shear-wave velocity profiles (EPRI, 1993; Silva et al., 1997). Profile depth (depth to competent material) is also varied on a site specific basis using a uniform distribution. The depth range is generally selected to reflect expected variability over the structural foundation as well as uncertainty in the estimation of depth to competent material.

To model parametric variability for compression-waves, the base-case Poisson's ratio is generally fixed. Suites of compatible random compression- and shear-wave velocities are then generated based on the random shear-wave velocities profiles.

To accommodate variability in modulus reduction and hysteretic damping curves on a generic basis, the curves are independently randomized about the base case values. A log normal distribution is assumed with a σ_{ln} of 0.35 at a cyclic shear strain of 3 x 10^{-2}%. These values are based on an analysis of variance on a suite of laboratory test results. An upper and lower bound truncation of 2σ is used to prevent modulus reduction or damping models that are not physically possible. The random curves are generated by sampling the transformed normal distribution with a σ_{ln} of 0.35, computing the change in normalized modulus reduction or percent damping at 3 x 10^{-2}% shear strain, and applying this factor at all strains. The random perturbation factor is reduced or tapered near the ends of the strain range to preserve the general shape of the median curves (Silva, 1992).

To model vertical motions, incident inclined compression- and shear (SV)-waves are assumed. Raytracing is done from the source location to the site to obtain appropriate angles of incidence. In the P-SV site response analyses, linear response is assumed in both compression and shear with the low-strain shear-wave damping used for the compression-wave damping (Johnson and Silva, 1981). The vertical and horizontal motions are treated independently in separate analyses. Validation exercises with a fully 3-D soil model using recorded motions up to 0.50%g showed these approximations to be validate (EPRI, 1993).

In addition, the site response model for the vertical motions has been validated at over 100 rock and soil sites for three large earthquakes: 1989 **M** 6.9 Loma Prieta, 1992 **M** 7.2 Landers, and the 1994 Northridge earthquakes. In general, the model performs well and captures the site and distance dependency of vertical motions over the frequency range of about 0.3 to 50.0 Hz and the fault distance range of about 1 to 100 km.

APPENDIX B

REFERENCES

Electric Power Research Institute (1993). "Guidelines for determining design basis ground motions." Palo Alto, Calif: Electric Power Research Institute, vol. 1-5, EPRI TR-102293.

vol. 1: Methodology and guidelines for estimating earthquake ground motion in eastern North America.
vol. 2: Appendices for ground motion estimation.
vol. 3: Appendices for field investigations.
vol. 4: Appendices for laboratory investigations.
vol. 5: Quantification of seismic source effects.

Iwan, W.D. (1967). "On a class of models for the yielding behavior of continuous and composite systems." *J. Appl. Mech.,* 34, 612-617.

Johnson, L.R. and W.J. Silva (1981). "The effects of unconsolidated sediments upon the ground motion during local earthquakes." *Bull. Seism. Soc. Am.*, 71, 127-142.

Schnabel, P.B., J. Lysmer, and H.B. Seed (1972). *SHAKE: a Computer Program for Earthquake Response Analysis of Horizontally Layered Sites.* Earthq. Engin. Res. Center, Univ. of Calif. at Berkeley, EERC 72-12.

Schneider, J.F., W.J. Silva, and C.L. Stark (1993). Ground motion model for the 1989 **M** 6.9 Loma Prieta earthquake including effects of source, path and site. *Earthquake Spectra,* 9(2), 251-287.

Seed, H.B. and I.M. Idriss (1970). "*Soil Moduli and Damping Factors for Dynamic Response Analyses,"* Earthq. Eng. Res. Center, Univ. of Calif. at Berkeley, Report No. UCB/EERC-70/10.

Silva, W.J., N. Abrahamson, G. Toro, and C. Costantino (1997). "Description and validation of the stochastic ground motion model." Submitted to Brookhaven National Laboratory, Associated Universities, Inc. Upton, New York.

Silva, W.J. (1992). "Factors controlling strong ground motions and their associated uncertainties." *Dynamic Analysis and Design Considerations for High Level Nuclear Waste Repositories, ASCE* 132-161.

Silva, W. J., T. Turcotte, and Y. Moriwaki, (1988). "Soil Response to Earthquake Ground Motion," Electric Power Research Institute, Walnut Creek, California, Report No. NP-5747.

Silva, W.J. (1976). "Body Waves in a Layered Anelastic soilid." *Bull. Seis. Soc. Am.*, vol. 66(5), 1539-1554.